~~Assessing the drought resilience of different land management scenarios using a tracer-aided ecohydrological model with variable root uptake distributions~~

~~Assessing /~~ **Exploring** impacts of **forest management** strategies~~impacts~~ **on water partitioning** in~~and~~ **a drought**-sensitive catchment~~resilience~~ **using a tracer-aided ecohydrological framework**

Cong Jiang [1], Doerthe Tetzlaff [1, 2, 3], Songjun Wu[1], Christian Birkel [1, 4], Hjalmar Laudon [5], Chris Soulsby [1, 3, 5, 6]

[1] Leibniz-Institute of Freshwater Ecology and Inland Fisheries (IGB), Department of Ecohydrology and Biogeochemistry, Berlin, Germany
[2] Department of Geography, Humboldt University Berlin, Berlin, Germany
[3] Northern Rivers Institute, University of Aberdeen, Aberdeen, UK
[4] Department of Geography, University of Costa Rica, San Pedro, Costa Rica
[5] Department of Forest Ecology and Management, Swedish University of Agricultural Science (SLU), Sweden
[6] Chair of Water Resources Management and Modeling of Hydrosystems, Technical University Berlin, Berlin, Germany

Correspondence to: Cong Jiang (cong.jiang@igb-berlin.de)

Abstract. Land use strongly influences water partitioning, water availability, and ecohydrological resilience in drought-sensitive regions. Forest management plays a critical role through its effects on water use, which depend~~s~~ on forest type~~species composition~~, forest ~~stand~~ density, root~~ing~~ water uptake~~depth, canopy structure, and age~~. ~~However~~, yet the ecohydrological consequences of different forest management strategies—particularly in terms of blue and green water fluxes—remain poorly quantified ~~for land use planning~~. Here, we develop and apply a parsimonious, tracer-aided forest management scenario framework using the conceptual ecohydrological model EcoPlot-iso, designed to isolate the dominant vegetation-structural controls on long-term water partitioning. ~~This study conducted a series of modelling experiments using the tracer-aided conceptual ecohydrological model EcoPlot-iso as a decision-support tool.~~ We investigated how variations in generic forest type (e.g., broadleaf vs. conifer), forest density, and root distribution influence water partitioning and ecohydrological resilience under different wetness conditions in the drought-sensitive lowland Demnitzer Millcreek catchment (DMC), northeastern Germany. Baseline simulations for the period (2000–2024) ~~across~~ were conducted at three forest sites~~several land use types~~ and ~~were~~ used to develop ~~a~~ forest-type–specific reference conditions ~~forest~~ for comparison with alternative forest management scenarios. A key innovation in this version of EcoPlot-iso was the integration of a depth-dependent root water uptake function, allowing simulation of transpiration across soil layers ~~across forests~~ with contrasting ~~different~~ rooting distribution , and stand ages~~, and species compositions~~. The model was calibrated and validated using seven years of soil moisture and three years of soil water isotope (δ^2H) data through a multi-criteria approach.

Results showed that, on average, evapotranspiration was ~~8% higher under conifers than broadleaf forests, and 12% higher than agroforestry. Agroforestry, in contrast, provided the highest groundwater recharge—11% and 4% more than conifers and broadleaf forests, respectively.~~ highest under conifers, exceeding broadleaf forests and

Formatted: Add space between paragraphs of the same style, Don't snap to grid

Formatted: Add space between paragraphs of the same style, Don't snap to grid

agroforestry by 7% and 11%, respectively, while agroforestry exhibited the greatest groundwater recharge. Significant differences in water partitioning between dry and wet years were observed across management scenarios. Comparisons between wet and dry years indicate that conifer forests show the strongest transpiration contrasts relative to broadleaf forests in early spring, while peak drought sensitivity occurs in late spring. Our findings highlight the potential of agroforestry, such as crop–tree mixtures, to mitigate drought impacts. Overall, this study demonstrates how a parsimonious, tracer-aided scenario framework can be used as a decision-support tool ~~The modelling framework provides a means~~ to quantify and ~~visualise~~visualize the effects of land use change on water availability in data-limited regions, supporting more informed decision-making ~~for~~ and enhanced ecohydrological resilience~~t~~ under increasing drought pressure~~land and water management~~.

1 Introduction

Land use plays a crucial role in regulating water, carbon, energy, and nutrient cycles by mediating ecohydrological fluxes and soil water storage dynamics which link interactions between the atmosphere, soils, vegetation and biogeochemical processes (Mahmood et al., 2014; Pielke et al., 2011; Smith et al., 2021; Sterling et al., 2013). Among the different types of land cover, forests are particularly important elements of the land use mosaic, providing a range of ecosystem services, including enhancing infiltration, stabilizing soils, storing carbon, supplying timber and fuelwood, as well as buffering extreme climate events (Bonan, 2008). However, there are clear trade-offs, as forests and trees also tend to use more water than contrasting land uses (Bosch & Hewlett, 1982; Calder, 1998). This is because their high Leaf Area Index (LAI) and canopy storage capacities often result in greater interception losses and canopy evaporation, while their deeper and denser rooting networks can sustain transpiration when top soils dry out (Wang-Erlandsson et al., 2014). Consequently, forest management decisions, (e.g., afforestation, thinning, forest type ~~species~~ selection etc.) can significantly affect water yield, the partitioning into blue (runoff, groundwater recharge) and green (evapotranspiration) water fluxes, and ~~overall~~ the ~~drought~~ ecohydrological resilience to drought~~;~~ ~~–~~defined here as the ability of soil–plant–water system to sustain key hydrological and ecological functions under drought stress (Falkenmark & Rockström, 2006; Neill et al., 2021; Tetzlaff et al., 2024).

Formatted: English (United States)

Formatted: English (United States)

Sustainable land management also requires consideration of sensitivity to climate change, which is altering hydroclimatic regimes by shifting precipitation patterns~~,~~ and increasing~~rising~~ atmospheric moisture demand~~intensifying drought frequency and duration in many areas~~ (Huntington, 2006; Trenberth, 2011). These changes can intensify drought frequency and duration, increase ~~increase atmospheric demand and~~ evaporative losses, and reduc~~ing~~ groundwater recharge and surface water availability, and thus exacerbating water scarcity in many regions (Ault, 2020; Yuan et al., 2023). Because ~~As~~ land use practices—particularly forest management—are expected to strongly influence water partitioning, it is important to ~~understanding~~ assess their impacts under changing hydroclimatic conditions in order ~~is essential for maintaining~~to evaluate the ecohydrological resilience of ~~nt~~ soil–plant–water ~~water and land~~ systems, especially in drought-~~prone~~ sensitive areas.

The understanding ofs ~~on~~ how land use change affects runoff generation, soil moisture storage and evapotranspiration dynamics has~~ve been~~ gradually developed through decades of research, including long-term paired experimental watershed investigations of~~studies such as paired catchment experiments on~~ water yield (Bosch & Hewlett, 1982; Brown et al., 2005, 2013; Hibbert, 1967). However, quantifying the impact of forest management on water partitioning remains challenging in most situations (Guswa et al., 2020). This is due to the complex interplay of climate conditions, soil properties, vegetation type, and topography, and the difficulty in distinguishing individual evapotranspiration (ET) ~~ET~~ components (Kool et al., 2014; Smith et al., 2021; Zhang et al., 2001). These challenges are further compounded by scarce long-term observational data for forest ecosystems, which are essential given their slow dynamics and lengthy growth cycles (Tetzlaff et al., 2017).

In forest ecosystems, ET is particularly challenging ~~difficult~~ to simulate due to complex interactions among canopy structure, stomatal behavior, and root water uptake (Tague & Band, 2004). ~~Although m~~Many ecohydrological models include some form of root water uptake parameterization ~~conceptualization~~ (e.g., mHM, EcH2O-iso), in which canopy transpiration is typically constrained by surface energy balance and stomatal conductance and subsequently distributed among soil layers based on soil water availability and root distribution. While such models provide detailed representations of land–atmosphere and soil–vegetation interactions, their application in forest management studies is often constrained by high data requirements, computational demand, and parameter uncertainty, particularly in data-scarce regions (Fatichi et al., 2012; Ricci et al., 2020; Tague & Band, 2004). In this context, conceptual tracer-aided ecohydrological models can provide a complementary, process-based, and practical framework for systematically exploring long-term forest management impacts on water partitioning and ecohydrological resilience (Landgraf et al., 2023). By integrating climatic forcing, canopy structure (e.g., leaf area index), soil moisture dynamics, and stable water isotopes, such approaches facilitate robust assessment of green- and blue-water fluxes under contrasting forest management scenarios (Neill et al., 2021).

In this study, we apply the tracer-aided conceptual model EcoPlot-iso to assess how land use, ~~–~~specifically forest management strategies,~~ –~~ influences water partitioning and soil moisture storage in the drought-sensitive, lowland Demnitzer Millcreek catchment, NE Germany. Thise lowland catchment is typical of large areas in central Europe where freely draining, sandy soils combine with a relatively low precipitation, and high evaporative demand amplify drought stress under climate change~~dry and warm climate to limit water availability~~. To improve the quantification of transpiration, we introduce a novel development in EcoPlot-iso by integrating a depth-dependent root water withdrawal function into the transpiration equation. The model is dual-calibrated and validated using seven years of soil moisture data and three years of soil water isotope data. A series of generic forest management scenarios_—_varying ~~in~~ broad ~~forest density, canopy structure~~ forest types (broadleaf~~deciduous~~, coniferous, agroforestry), forest density, and rooting characteristics_—_are developed within a parsimonious, tracer-aided forest management scenario framework, to explore their impacts on vertical water fluxes and ecohydrological resilience.

This study aims to answer the following research questions:

- How does vegetation cover influence water use and partitioning under varying wetness conditions in a drought-sensitive, lowland catchment?

Formatted: English (United States)

- What are the implications of alternative generic forest management scenarios for water availability and overall ecohydrological resilience?
- How can we optimize the land management strategies to mitigate drought impacts and enhance ecohydrological resilience in the face of climate change?

2 Study area

2.1 Demnitzer Millcreek catchment (DMC)

The Demnitzer Millcreek catchment (DMC) is a 66 km² lowland basin (30–90 m elevation) in the State of Brandenburg, Germany, approximately 55 km east of Berlin (52°23′ N, 14°15′ E) (Fig.~~ure~~ 1). Located in the Northern European Plain, it is part of a drought-sensitive region that provides many essential ecosystem services, including agriculture, timber production, and water supply.

The DMC landscape is dominated by non-irrigated farmland, mostly arable crops and some grazing on more water-retentive soils brown and gley soils respectively which cover 60% of the catchment ~~in the~~ (Fig. 1a and b). Forests cover 36% of the catchment on more freely draining sandy soils, and include coniferous, broadleaf, and mixed stands. Small urban settlements (2%) are scattered throughout the catchment, with wetlands on peat soils primarily found along streams in the central part of the catchment. The climate is temperate with warm summers, with a mean annual temperature of 9.6°C and average precipitation of approximately 558 mm, based on weather station data from 2000 to 2024 ~~(see Table 2)~~. Potential evapotranspiration (PET) ranges from 584 to 789 mm per year from 2000 to 2024, based on calculations from this study (see Section 3.3~~Table 2~~). Interannual variability in precipitation, including the identification of dry and wet years, is shown in Fig.~~ure~~ S~~3~~1, which highlights deviations from the long-term mean and helps contextualize recent drought impacts. Rainfall peaks in summer, accompanied by intense convective storms; however, surface runoff is rare, as the soils are highly permeable and dry in the growing season. Consequently, the catchment is primarily groundwater-dominated with winter high flows and often dries in the summer (Smith et al., 2021). The geology consists mainly of glacial and fluvial deposits and base moraines, while the dominant soil types include poorly drained silty gley brown earth and well-drained podzolic brown earth soils (Fig.~~ure~~ 1b).

The DMC has a long history of human influence, with significant land use changes affecting its hydrology. In the 18th Century, artificial drainage channels were constructed to convert wetlands into agricultural land. Since the 1990s, efforts in wetland restoration and wildlife recolonization (e.g., beaver recovery) have aimed to enhance water retention in the landscape. Long-term hydrological and isotopic monitoring (Gelbrecht et al., 1996, 2005; Smith et al., 2020; Wu et al., 2021) has provided valuable insights into the impacts of agriculture and land use management on water quality, ecohydrological partitioning and soil water storage. The 2018 European drought and subsequent prolonged dry periods have exacerbated water scarcity and ecosystem vulnerability (Kleine et al., 2021). In response, some land owners have explored agroforestry and other adaptive forest and tree management strategies to improve water retention and landscape resilience (Luo et al., 2024). Agroforestry represents a transitional system blending low density tree cultivation and with agriculture; either in terms of grazing the understory vegetation or crops (Landgraf et al., 2022; Quandt et al., 2023). ~~Such systems are characterized by minimal canopy cover and no artificial irrigation, though mulching is often used to enhance soil moisture storage.~~

~~Such systems typically involve rows of small deciduous trees or shrubs (≤2 m in height), spaced 2–3 m apart, interplanted with rainfed legumes (Landgraf et al., 2023).~~ Given the long-term monitoring record and ongoing land use change, DMC serves as a useful site for assessing the impacts of changing forest management on water partitioning, soil moisture and ecohydrological resilience under different wetness conditions.

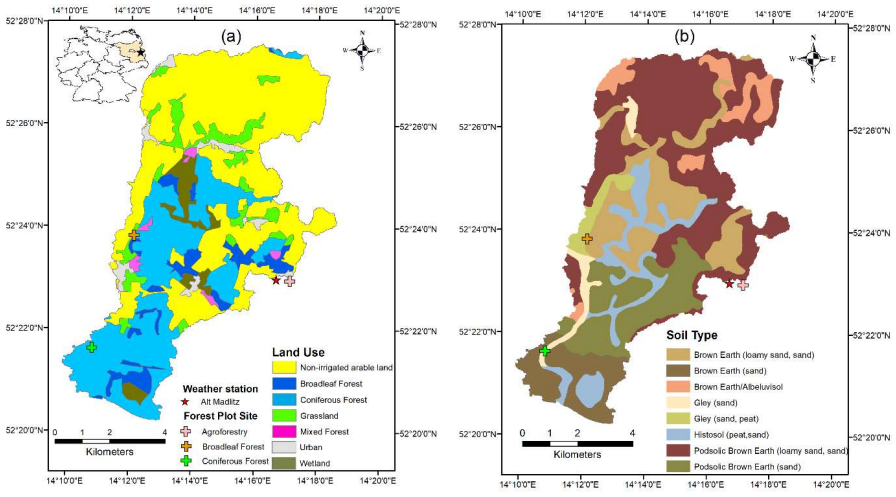

Figure 1. Location, land use (a) and soil type (b) map of the Demnitzer Millcreek catchment, showing the current distribution of broadleaf forests, conifer forests, agroforestry, cropland, and grassland.

2.2 Forest Plot Sites

To investigate the effects of forest management scenarios on water partitioning and ecohydrological resilience, ~~a~~ three ~~monitoring~~ predominantly ~~broadleaf~~ forest plot sites — broadleaf forest, conifer forest and agroforestry — ~~wereas~~ selected within the drought-sensitive DMC ~~in the northeastern NE Germany~~. ~~This~~ These plots represents ~~a~~ contrasting ~~key~~ forest type central to the modelling experiments. ~~: a relatively mature (~60 years old) broadleaf forest system. Moreover, it is formed on the extensive freely draining sandy brown soils that are particularly drought sensitive in DMC due to their poor water retention characteristics.~~ The plot locations ~~is~~are shown in Fig.~~ure~~ 1, and key site characteristics are ~~descripted~~ summarized below, with ~~more~~ further details available in Kleine et al. (2021) and Landgraf et al. (2023). A summary of observed soil types and soil moisture monitoring characteristics for these three forest sites is provided in Table 1, which also highlights pronounced differences in long-term mean volumetric soil moisture averaged over the 0–1 m soil profile, with values highest in agroforestry (~21%), intermediate in broadleaf (~11%), and lowest in conifer forest (~5.5%).

~~Specifically, t~~The broadleaf forest site represents a relatively mature forest system (~60 years old) and is dominated by mature European oak (Quercus robur) with a few Scots pine (Pinus sylvestris) present within the

Formatted: Indent: Left: 0"

Formatted: English (United States)

Formatted: English (United States)

plot. Additional species including Norway maple (Acer platanoides), elm (Ulmus spp.), and hazel (Corylus avellana) are found within 10 m of the plot boundary. The soil is classified as Brown Earth, with a loamy sand to sand texture. ~~The soil is a freely draining Lamellic Brunic Arenosol (Humic), characterized by loamy sand to sand textures. This corresponds to a typical brown earth in regional classification systems.~~

The conifer forest site is structurally simpler and more homogeneous, and is dominated by mature Scots pine (Pinus sylvestris) plantation. A limited number of broadleaf species, such as European oak and Norway maple, are also present within the plot, reflecting a ~~mixed but~~ conifer-dominated canopy. The soil is a weakly developed brown earth~~classified as a Gley (sand)~~, characterized by coarse sandy texture and overlying gravels~~locally compacted conditions at depth~~.

The agroforestry site represents a transitional system between forest and agriculture and is characterized by minimal canopy cover and no irrigation. It consists of rows of small deciduous trees or shrubs (≤2 m in height), spaced approximately 2–3 m apart, interplanted with rainfed legumes (Landgraf et al., 2023). The soil is classified as pPodsolic bBrown cEarth, with a loamy sand to sand texture.

Together, these three sites represent a realistic gradient of forest land use intensity and provide a basis for exploring how forest type, forest density, and rooting depth affect ecohydrological responses under varying climatic conditions.

~~**Table 1.** Summary observed soil type and soil moisture at three forest sites.~~

~~Site~~	~~Soil Type~~	~~Texture~~	~~Layer~~	~~Soil Moisture (mm)~~			
				~~Max~~	~~Min~~	~~Mean~~	~~SD~~
~~Broadleaf forest~~	~~Brown Earth~~	~~Loamy sand/sand~~	~~0 to 10 cm~~	~~26.28~~	~~3.50~~	~~13.67~~	~~6.30~~
			~~10 to 30 cm~~	~~56.19~~	~~6.86~~	~~24.68~~	~~11.70~~
			~~30 to 100 cm~~	~~147.51~~	~~25.83~~	~~71.71~~	~~33.50~~
			~~10 to 30 cm~~	~~53.35~~	~~7.15~~	~~29.75~~	~~13.49~~
			~~30 to 100 cm~~	~~223.62~~	~~86.83~~	~~163.41~~	~~41.98~~

Table 1. Summary of observed soil types and soil moisture data at the three forest sites.

Site	Soil Type	Texture	Layer	Soil Moisture (mm)				Period
				Max	Min	Mean	SD	
Broadleaf forest	Brown cEarth	Loamy sand/sand	0 to 10 cm	26.3	3.5	13.7	6.3	2018.6-2024.12
			10 to 30 cm	56.2	6.9	24.7	11.7	
			30 to 100 cm	147.5	25.8	71.7	33.5	
Conifer forest	Sandy brown earth~~Gley (Sand)~~	Coarse sand ~~Sand, compacted~~	0 to 10 cm	28.7	8.6	17.3	7.1	2019.3-2024.12
			10 to 30 cm	53.8	2.6	21.8	12.3	
			30 to 100 cm	34.7	2.7	15.9	8.0	
Agroforestry	Podsolic bBrown cEarth	Loamy sand/sand	0 to 10 cm	32.1	10.4	21.3	7.8	
			10 to 30 cm	53.4	7.2	29.8	13.5	
			30 to 100 cm	223.6	86.8	163.4	42.0	

Formatted ... [1]
Formatted ... [2]
Formatted ... [5]
Formatted ... [6]
Formatted ... [7]
Formatted ... [8]
Formatted ... [9]
Formatted ... [10]
Formatted ... [11]
Formatted ... [12]
Formatted ... [3]
Formatted ... [4]
Formatted ... [13]
Formatted ... [14]
Formatted ... [15]
Formatted ... [16]
Formatted ... [17]
Formatted ... [18]
Formatted ... [19]
Formatted ... [20]
Formatted ... [21]
Formatted ... [22]
Formatted ... [23]
Formatted ... [24]
Formatted ... [25]
Formatted ... [26]
Formatted ... [27]
Formatted ... [28]
Formatted Table ... [29]
Formatted ... [32]
Formatted ... [33]
Formatted ... [34]
Formatted ... [35]
Formatted ... [30]
Formatted ... [36]
Formatted ... [37]
Formatted ... [38]
Formatted ... [39]
Formatted ... [31]
Formatted ... [40]
Formatted ... [41]
Formatted ... [42]
Formatted ... [43]
Formatted ... [48]
Formatted ... [49]
Formatted ... [50]
Formatted ... [51]
Formatted ... [52]
Formatted ... [53]
Formatted ... [54]
Formatted ... [55]
Formatted ... [44]
Formatted Table ... [45]
Formatted ... [47]
Formatted ... [46]
Formatted ... [56]
Formatted ... [57]

3 Method and Data

3.1 Model Framework and Structure

This study employs the EcoPlot-iso model, a tracer-aided ecohydrological modelling framework designed to simulate key ecohydrological and isotopic processes ~~transformations~~ that characterise water partitioning at the plot scale (Birkel et al., 2024; Landgraf et al., 2023; Stevenson et al., 2023). EcoPlot-iso is a process-based conceptual model that simulates key ecohydrological fluxes, including interception, throughfall, infiltration, preferential flow, surface runoff, percolation, and groundwater recharge, as well as evapotranspiration components such as canopy evaporation, soil evaporation, and transpiration (Fig.~~ure~~ 2a). These processes are represented within a vertical structure comprising a single canopy layer and three soil layers (0–10 cm, 10–30 cm, and 30–100 cm) (Fig.~~ure~~ 2b). The vertical discretization follows the established EcoPlot-iso configuration and effectively represents vertical gradients in soil moisture and isotopic composition, broadly consistent with ~~support from~~ soil moisture and isotope measurements within each layer. Recently, the isotope tracking module was further developed to include fractionation and mixing processes, allowing EcoPlot-iso to better constrain the partitioning between ~~differentiate~~ evaporation ~~from~~ and transpiration and improve water flux estimates. The required input variables (Table 2) include meteorological data such as precipitation, potential evapotranspiration (PET), air temperature, and relative humidity, along with stable water isotopic data (precipitation isotope) and vegetation-related parameters (leaf area index, LAI).

In EcoPlot-iso, canopy surface cover fraction (SCF) is derived from LAI using Beer's law with an extinction coefficient γE (Eq. S1). Maximum canopy storage is determined by the SCF and an interception threshold parameter α. Interception is represented by a nonlinear saturation-type function (Eq. S2), whereby precipitation is first stored in the canopy until maximum canopy storage is reached, and any excess is routed as throughfall. Potential evapotranspiration PET is partitioned into canopy and soil fractions according to SCF (Eqs. S3 and S4). The canopy fraction drives evaporation from the interception store and transpiration from the soil layers, while the soil fraction drives evaporation from the upper soil layer (Eqs. S5–S6). Actual fluxes are constrained by water availability: interception evaporation depends on canopy storage, transpiration is sequentially satisfied from the upper to deeper soil layers according to the relative soil-moisture availability (STO/Smax) of each layer (Eqs. S7–S9), and soil evaporation is limited by moisture availability in the upper soil. Surface runoff is represented using a Hortonian threshold approach, where precipitation in excess of infiltration capacity is routed as runoff (Eq. S10). Preferential flow is triggered when throughfall exceeds a threshold, with a calibrated parameter controlling the bypass proportion (Eq. S11). Percolation, compartment flow and groundwater recharge are represented as storage–discharge relationships, where outflows are parameterised as power functions of soil or groundwater storage (Eqs. S12-S14). Groundwater recharge is defined as the downward percolation flux at the lower boundary of the soil domain (30–100 cm layer), corresponding to a total soil depth of 1 m. Full variable definitions and governing equations are provided in Table S~~2~~1 of the Supplementary Material (Eqs. S1–S14).

EcoPlot-iso has been applied in diverse climatic and hydrological settings, including a one-year simulation in Scotland (Stevenson et al., 2023), a one-year simulation at the Demnitzer Millcreek (DMC) site in the Northern European Plain (Landgraf et al., 2023), and a four-year simulation in the humid tropics of Costa Rica (Birkel et al., 2024).– Building on these applications, this study employs EcoPlot-iso for a long-term tracer-aided

Formatted: Font: Italic

Formatted: Font: Italic

ecohydrological simulation to assess the effects of different forest management scenarios on water partitioning and ecohydrological resilience.

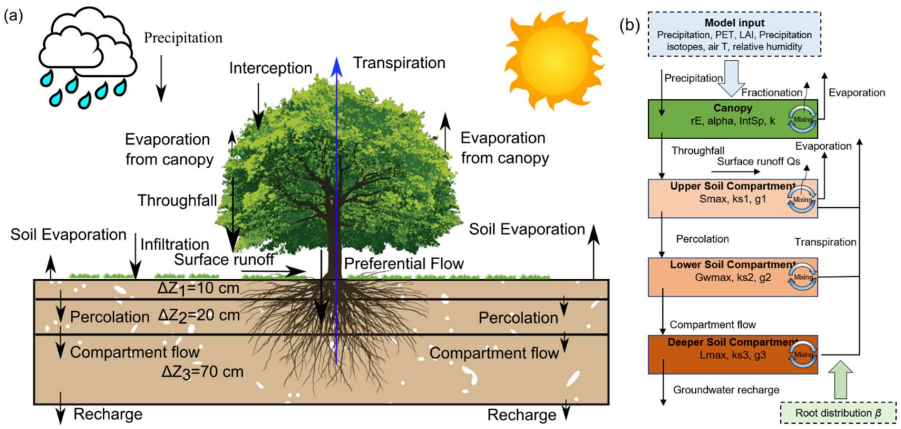

Figure 2. (a) Schematic representation of the ecohydrological fluxes and water partitioning in the EcoPlot-iso model illustrating major water fluxes and storage components; (b) Conceptual framework and key parameters of the EcoPlot-iso model(Landgraf et al., 2023; Stevenson et al., 2023), highlighting the key ecohydrological processes simulated in this study.

3.2 Model Adaptations: Integrating Root Distribution into the Transpiration Equation

Although root water uptake plays a critical role in soil–plant–atmosphere interactions, the vertical rooting distribution and the associated depth-dependent uptake efficiency ~~it~~ was not explicitly represented in EcoPlot-iso (Stevenson et al., 2023) The currentis study introduces a novel depth-dependent root uptake function to improve the model's simulation of transpiration and water partitioning across different root distributions. This adaptation enables the model to account for variations in rooting depth and water uptake efficiency across land use types—such as young and mature forests or contrasting vegetation covers—that affect soil water extraction. Specifically, a new transpiration equation was implemented to calculate root water uptake across three soil compartments—shallow, middle, and deep—by incorporating depth-specific uptake efficiency:

$$T_{p1} = r_{L1} * \left(T_P - E_i\right) * \left(\frac{STO}{S_{\max}}\right) \quad (1)$$

$$T_{p2} = r_{L2} * \left(T_P - E_i - T_{p1}\right) * \left(\frac{GW}{GW_{\max}}\right) \quad (2)$$

$$T_{p3} = r_{L3} * \left(T_P - E_i - T_{p1} - T_{p2}\right) * \left(\frac{SDeep}{SDeep_{\max}}\right) \quad (3)$$

where T_{p1}, T_{p2}, T_{p3} represent the transpiration from the upper, lower, and deeper soil compartments, respectively. E_i denotes the canopy evaporation. STO, GW, $SDeep$ represent the water storage in the upper, lower, and deeper soil compartments. S_{max}, GW_{max}, $SDeep$~~L~~$_{max}$ are the maximum water storage capacities of these compartments. ~~r~~$_{L1}$,

Formatted: Font: Italic

r_{L2} and r_{L3} represent the root water withdrawal efficiency in the upper, lower, and deeper soil compartments, respectively.

To explicitly link root water uptake to soil moisture availability and transpiration demand, an efficiency factor $r(z)$ was introduced. The exponential root water withdrawal efficiency function is defined as:

$$r(z) = e^{-\beta z} \quad (4)$$

Field Code Changed

where $r(z)$ represents the capacity of roots to extract water at depth z, and β is the decay rate, which determines how quickly root activity decreases with increasing depth. A higher β value concentrates root activity near the surface, while lower β values allow for deeper water uptake (see ~~Supplement~~ Fig.~~ure~~ S2 in Supplement~~1~~). This formulation builds on the common assumption that potential root water uptake decreases exponentially with depth (Li et al., 1999; Wu et al., 1999) and is intentionally simplified for a plot-scale, data-constrained model setup. The soil profile is discretized into three layers (0–10 cm, 10–30 cm, and 30–100 cm; Fig. 2a), and rL1, rL2, and rL3 are calculated by evaluating r(z) at the midpoint depth of each layer (z = 5, 20, and 65 cm, respectively). These layer-specific efficiency values are then used as weighting coefficients in Eqs. (1)–(3) to calculate transpiration from each of the three soil compartments.

3.3 Model Setup and Input and Observation Data

The EcoPlot-iso model was applied to DMC across ~~four~~ five sites with different dominant land use: broadleaf forest, conifer forest, ~~cropland,~~ agroforestry, cropland and grassland over a 25-year period (2000–2024) at daily timesteps. Soil moisture initialization was based on observed data, and a one-year spin-up period was included before each simulation to stabilize initial conditions. The input datasets required for the model—climate, vegetation, soil moisture, and stable water isotope data—are summarized in Table 2. Climate variables, including precipitation, temperature, wind speed, and relative humidity, were primarily obtained from the Müncheberg weather station (DWD, German Weather Service, ~20 km from DMC). Potential Evapotranspiration (PET) was calculated using the FAO Penman-Monteith equation, while net radiation was derived from ERA5 reanalysis data (Hersbach et al., 2020). The Leaf Area Index (LAI) time series was extracted ~~obtained~~ from the MODIS 8-day LAI product ~~resolution dataset~~ at the location of each study site and linearly interpolated to daily timesteps. To improve accuracy and reduce data noise, the MODIS LAI was further bias-corrected against in-situ ~~adjusted using in-situ~~ LAI measurements (maximum and minimum values), following ~~(~~Smith et al.~~,~~ (2021) and~~;~~ Wu et al.~~,~~ (2023). Given the plot-scale setup of EcoPlot-iso, agroforestry systems, characterized by mixed crop–tree vegetation, are represented implicitly using MODIS-derived LAI and calibration against plot-scale soil moisture and isotope observations, rather than explicitly resolving multiple vegetation types. In addition, ~~T~~the complete set of time series input data used to drive the EcoPlot-iso simulations in the Demnitzer MillCreek Catchment for 2000-2004—including daily precipitation, precipitation isotopes (δ^2H), air temperature, relative humidity, Leaf Area Index (LAI), and potential evapotranspiration (PET)—is presented in Figure S32 of the Supplementary Material.

Surface soil moisture (0–10 cm) was measured using a handheld soil moisture device (Theta handheld probe ML3 Sensor) on a monthly basis during two field observation periods ~~of more detailed observations (in~~ 2018–2019 and ~~in~~ 2021). For subsurface soil moisture, permanently installed soil moisture probes: SMT-100 at forest and grassland sites, and CS650 at agroforestry and cropland sites. Measurements were recorded at 15-minute intervals

with two replicates per depth. ~~(two replicates at each depth) were used to continuously monitor Volumetric Water Content (VWC) at 15-minute intervals at four sites (Figure 1).~~ To facilitate data processing and consistency, all soil moisture datasets were aggregated into daily mean values, resulting in one volumetric water content ~~VWC~~ value per site and soil depth. ~~A~~ Details ~~summary~~ of the measurement devices, depth intervals, and aggregation methods is summarized in Table S~~1~~2. Daily precipitation samples for stable water isotope analysis from June 2018 onward were collected at the Hasenfelde AWS, and earlier data were obtained from the Berlin weather station. Soil water isotopes were sampled from bulk soil at the four plot sites at five depths (0–5, 5–10, 10–20, 20–30, and 30–50 cm) every 3–4 weeks during the growing season. The isotope data were aggregated according to the thickness of the corresponding model soil compartments. All isotope values are reported relative to Vienna Standard Mean Ocean Water (VSMOW). Further details on site instrumentation and data collection are described in Landgraf et al. (2022).

Table 2. Summary of the used climate, vegetation, soil moisture, and isotope data.

Data	Unit	Period	Timestep	Acquisition
Climate data				
Precipitation	mm/d	2000-2024	Daily	Muencheberg weather station (52.52°, 14.12 °)
Temperature	°C			
Windspeed	m/s			
Relative humidity	%			
Net shortwave radiation	W/m^2		Hourly	ERA5
Net longwave radiation				
Potential evapotranspiration	mm/d		Daily	FAO Penman-Monteith equation
Vegetation data				
Leaf area index	-	2000-2024	8-days	MODIS at broadleaf forest, coniferous, and agroforestry sites
Soil data				
Soil moisture	%	2018-2024	Daily	broadleaf forest, cropland, agroforestry, and grassland sites
Isotope data				
Precipitation isotope δ^2H	‰	2000-2024	Daily	Hasenfelde (52.41°N, 14.19°E), weather station in Berlin
Soil water isotope		2018-2019, 2021	Daily	Manually at broadleaf forest, cropland, agroforestry, and grassland sites

Formatted: Line spacing: single, Don't snap to grid

3.4 Model Calibration and Validation

The EcoPlot-iso model was calibrated using the Monte Carlo ~~method~~ approach ~~and~~ combined with a multi-criteria ~~approach~~ evaluation based on soil moisture and soil water isotope ~~data~~ observations ~~for~~ at each land use site. For each ~~model~~ calibration~~run~~, ~~a total of~~ 100,000 parameter sets were generated using the Latin Hypercube Sampling (LHS) within a Monte Carlo framework (McKay et al., 1979) to broadly sample the parameter space and capture a wide range of plausible model behaviors.

The initial parameter ranges~~, representing the widest physically feasible values for the site,~~ were ~~determined~~ defined based on a literature ~~review~~ values and site-specific knowledge~~, with identical constraints applied across~~

~~all vegetation types~~. Specifically, initial ranges for the radiation extinction factor (γE) were guided by vegetation-specific light attenuation coefficients from canopy gap-fraction theory (Larcher, 1975; Gigante et al., 2009), using typical reference values of 0.35 for grasslands, 0.45 for croplands, and 0.65 for forests.

Initial ranges for the interception storage capacity parameter (α) were guided by scaling values reported in global syntheses of canopy interception storage (Zhong et al., 2022) and interception sensitivity studies (Barnard et al., 2014), accounting for differences in model time step and formulation. The resulting interception evaporation is consistent with observational studies indicating that canopy interception losses typically represent approximately 10–30% of annual precipitation in forested systems (Staelens et al., 2008; Llorens & Domingo, 2007).

Model performance was evaluated using the modified Kling-Gupta Efficiency (*mKGE*) (Kling et al., 2012), ~~optimizing~~ calculated separately for~~the averaged *mKGE* for~~ soil moisture ($mKGE_{sm}$) and soil water isotopes ($mKGE_{iso}$) ~~across~~ at ~~the~~ each of the three soil depth layers. ~~*(i)* to ensure robust parameter selection (Eq. 5).~~ Calibration followed a two-step refinement process**.** In the first step, based on the initial parameter ranges, parameter sets were retained only if they fell within the intersection of the top 60th percentile of all six individual *mKGE* metrics (i.e. soil moisture and soil water isotopes at each of the three soil depths)~~the top 60th percentile of best-performing simulations—ranked by average *mKGE*—along with their corresponding calibrated parameter sets, were retained~~. This intersection-based filtering ensured that retained simulations performed consistently well across all evaluated variables and depths. By retaining only the performance metrics and corresponding parameter sets, this step efficiently screened the parameter space while substantially reducing data storage requirements during the initial exploration.

In the second step, the model was re-run using the retained parameter space obtained from Step 1.; For these re-run simulations, an average *mKGE* value across depths and variables was then used as the objective performance metric (Eq. 5), and the 100 best-performing simulations were selected for final analysis.~~and the 100 best simulations were selected from the top 60th percentile to ensure optimal parameter selection.~~ The model parameters, their initial ranges, and the refined ranges for each of land use are summarized in Table S3 in the Supplement. To assess parameter constraints and equifinality, the probability density distributions and median values of the calibrated parameters were derived from the 100 best-performing simulations for each site (see Fig. S4). These were then used to evaluate the convergence of the parameters relative to their initial ranges.

$$mKGE = \frac{\sum_i^3 mKGE_{sm} + \sum_i^3 mKGE_{iso}}{6} \quad (5)$$

Model parameters were calibrated using the full available observation, comprising seven years of soil moisture data and three years of soil water isotope data, in order to maximise information content under limited isotope availability (Shen et al., 2022). To additionally assess model robustness beyond a shortter~~the~~ calibration window, a split-sample calibration–validation experiment was conducted consistently across all land-use types. In this experiment, the model was calibrated using an earlier subset of the soil moisture and isotope observations, followed by validation against an independent soil moisture period, as isotope observations were not available for validation. Results from this split-sample evaluation, which showed good paramater transferability across most sites, are reported in Table S4 and Figures S5–S7 of the Supplement. Given this transferability, t~~T~~he full-period calibration was retained for the main scenario simulations, as it provides more stable parameter estimates under

Formatted: Font: Italic

Formatted: Font: Italic

Formatted: Font: (Default) Times New Roman, (Asian) KaiTi, 10 pt

Formatted: Font: Italic

Formatted: English (United States)

Formatted: Font: Italic

Formatted: English (United States)

Formatted: Justified

data limitations, while the split-sample results are presented for transparency and robustness assessment.

3.5 Development and Application of a Generic Forest Management Scenario Framework

The primary goal of this study was to develop a new, parsimonious and generic forest management scenario framework to evaluate how forest type, forest density, and root distribution —associated with forest age— influence long-term water partitioning and ecohydrological resilience under comparable environmental conditions. This framework was designed to capture the dominant effects of vegetation structure—such as interception and transpiration through canopy and root networks—on water partitioning, rather than to reproduce detailed species-specific physiology.

~~To assess the general impacts of different forest management strategies on water partitioning and ecohydrological resilience, we developed a framework for quantifying generic forest management scenarios based on simulations at the broadleaved forest site at DMC.~~ Based on this conceptual framework, ~~B~~baseline simulations ~~(2000–2024)~~covering the period 2000-2024 were established using EcoPlot-iso model at ~~the broadleaf~~ three forest sites within the DMC (broadleaf forest, conifer forest, and agroforestry). These baseline simulations provide ~~–~~forest-type–specific reference conditions against which alternative management scenarios were evaluated.

To isolate the effects of forest management from site-specific soil properties and boundary conditions, we extended the observed forest-site configurations by systematically combining each forest-type–specific vegetation parameter with each site-specific soil parameter, resulting in a 3 × 3 scenario matrix (Fig. 3). The diagonal entries represent the observed site-based reference configurations—namely, Broadleaf forest site, Conifer forest site, and Agroforestry site —and are therefore treated as baseline scenarios. The remaining cross-combinations represent hypothetical but plausible forest-site (soil) configurations, in which vegetation characteristics are applied to alternative site-specific soil hydraulic properties and boundary conditions (e.g., soil texture and compaction). This design enables vegetation effects to be assessed independently of site-specific controls, while explicitly acknowledging that soil hydraulic properties and boundary conditions remain inherently site-dependent. Ensemble-based comparisons across site configurations for each forest type therefore support a more robust and generic interpretation of ecohydrological behhaviour.

Specifically,

~~From~~for ~~this~~ each of forest-site baseline scenario calibration, we retained the top 100 best-performing simulations—ranked by average ~~modified Kling-Gupta Efficiency (~~mKGE~~)~~—and their corresponding parameter sets (as described in Section 3.4). Forest-type–specific vegetation parameters (e.g., rE, α) were derived from site-specific calibrations for broadleaf, conifer, and agroforestry systems, and their median values from the 100 best-performing simulations at each site were used to represent characteristic vegetation conditions. The root distribution parameter (β) was not treated as strictly vegetation-specific, but as jointly influenced by vegetation type, soil properties, and soil water availability (Fig. S4). These calibrated parameter sets were then used for subsequent scenario simulations to ensure physically consistent parameter configurations across all forest types. In contrast, soil-related parameters (e.g., ks1, ks2, ks3, Smax, GWmax, Lmax) were retained from the corresponding forest sites to preserve site-specific hydraulic properties and boundary conditions. ~~These calibrated parameter sets were then used for scenario testing to ensure robust model performance across all simulations.~~

Formatted: English (United States)

Formatted: Font color: Auto

~~To isolate the effects of forest characteristics and management, all scenario simulations were driven using the same climate input data and precipitation isotope time series as the baseline, along with consistent forcing data for potential evapotranspiration.~~ ~~Additionally, site-specific Leaf Area Index (LAI) data were adjusted for the three forest types: broadleaf, coniferous, and agroforestry, which were derived from 8-day MODIS remote sensing products (2000–2024) (Table 2 and Figure S2d).~~For vegetation forcing, we used forest-type–specific observed LAI time series (broadleaf, coniferous, and agroforestry), derived from the MODIS LAI products, described in Section 3.3 (Table 2; Fig. S3d). Forest-type–specific initial soil moisture conditions for the three soil layers were kept consistent with the corresponding baseline simulations.

~~To isolate the effects of forest characteristics and management, a~~All scenario simulations were driven using identical climate input data, precipitation isotope time series, and potential evapotranspiration forcing as the baseline simulations to isolate the effects of forest characteristics and management.~~ll scenario simulations were driven using the same climate input data and precipitation isotope time series as the baseline, along with consistent forcing data for potential evapotranspiration.~~

The scenario framework varied three key dimensions of forest management:

~~a) Forest density was varied by multiplying the reference Leaf Area Index (LAI) by a scaling factor ranging from 0.2 to 1.8. Higher forest density was represented by scaling factors >1.0, indicating denser canopy cover, while lower forest density corresponded to factors <1.0, reflecting more open canopy conditions.~~

a) ~~Species~~ Forest type~~composition~~ was varied by implementing three canopy types—broadleaf, conifer, and agroforestry—each assigned type-specific LAI ~~values~~ time series ~~derived from MODIS data corrected using site data at DMC (see Section 3.3)~~ to reflect differences in ~~forest~~ canopy structure ~~and function~~.

Forest density was varied by multiplying the reference ~~Leaf Area Index (LAI)~~LAI by a scaling factor ranging from 0.2 to 1.8. Higher forest density was represented by scaling factors >1.0, indicating denser canopy cover, while lower forest density corresponded to factors <1.0, reflecting more open canopy conditions. The applied LAI scaling range (0.2–1.8) follows previous tracer-aided modelling approaches (Neill et al., 2021) and spans realistic management-induced variability in canopy density, while remaining consistent with reported LAI values for mature European forests (Leuschner et al., 2006).

b)

c) ~~Root water uptake efficiency was varied by parameterizing β values ranging from 0 to 2.0 to represent vertical root distribution. Lower β values indicated deeper rooting systems (e.g., older or deep-rooted species), while higher values represented shallower rooting systems (see Fig. S1).~~Root water uptake efficiency was varied by scaling the site-calibrated β parameter to represent contrasting vertical root distributions associated with forest developmental stage. Three rooting scenarios were considered: 0.5 × β, 1.0 × β, and 2.0 × β, where β is the calibrated value for each forest site. Lower scaled values (0.5 × β) represent more developed forests with deeper, less surface-weighted rooting systems, while higher scaled values (2.0 × β) represent younger or less-developed forests with shallower, more surface-weighted rooting distributions (see Fig. S1). The 1.0 × β scenario corresponds to the observed rooting distribution at each forest site.

Within this framework, LAI and rooting distribution were treated as independent scenario dimensions. LAI scaling represented management-induced changes in canopy density, whereas rooting distribution scenarios reflected

Formatted: Font: (Default) Times New Roman, (Asian) KaiTi, 10 pt

Formatted: Font: Italic

Formatted: Font: Italic

Formatted: Font: Italic

Formatted: Font: Italic

Formatted: Font: Italic

Formatted: Font: Italic

contrasts in belowground water uptake. Their combined effects on water fluxes were evaluated without assuming a fixed linkage between canopy structure and rooting depth. This separation acknowledges that canopy density can change rapidly through management (e.g., thinning or harvesting), while rooting characteristics typically reflect longer-term stand development, thereby allowing realistic representation of above- and belowground controls on water partitioning.

~~This generic and scalable framework enables systematic simulation of long-term forest management impacts on water partitioning, soil moisture dynamics, and ecohydrological resilience under consistent climatic conditions.~~ Although EcoPlot-iso was originally developed for plot-scale applications, it is applied here to represent ecohydrological fluxes in a range of well-characterized sites within the DMC region. The model employs a one-dimensional approach that does not explicitly account for lateral fluxes; however, this simplification is intentional. It enables clearer interpretation of process-level dynamics under contrasting vegetation and climate conditions, making it suitable for general scenario analysis. This assumption is especially justified in the DMC catchment, which is characterized by flat, lowland topography and is predominantly governed by vertical hydrological fluxes (Kleine et al., 2021; Smith et al., 2020).

~~The aim was not to reproduce exact spatial patterns, but to develop a generalizable understanding of how forest structure influences vertical water fluxes and soil moisture. The framework thus serves as a practical tool for assessing broad ecohydrological responses to forest management. Ultimately, the goal was to inform stakeholders of the potential impacts of changes in canopy structure and forest age on long-term water availability and ecohydrological resilience in drought-sensitive lowland catchments.~~The framework is not intended to reproduce exact spatial patterns or detailed species-specific physiology, but rather to capture the dominant effects of vegetation structure on vertical water fluxes and soil moisture dynamics. By focusing on variations in forest type, forest density, and root distribution associated with forest age and management, the framework enables a generalized assessment of long-term water partitioning and ecohydrological resilience under comparable environmental conditions. As such, it provides a practical and transferable tool for evaluating forest management impacts on water availability and ecohydrological resilience in drought-sensitive lowland catchments.

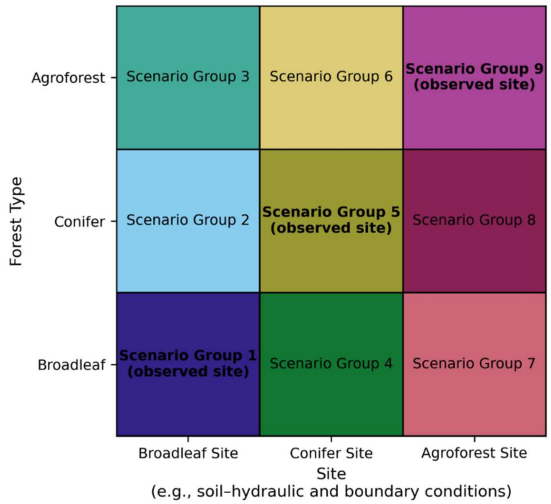

Figure 3. Matrix of nine Scenario Groups formed by combining three site-specific configurations (Broadleaf Site, Conifer Site, and Agroforest Site) with three forest types (Broadleaf, Conifer, and Agroforest). Each colored block represents a Scenario Group consisting of multiple sub-scenarios (e.g., varying forest densities and root water uptake distributions). Diagonal entries (Scenario Groups 1, 5, and 9), marked as "observed configuration", correspond to forest–site combinations observed at the field sites, where vegetation type and site-specific soil–hydraulic and boundary conditions are consistent with real-world conditions.

Formatted: Font: Bold

4 Results

4.1 Dynamics of Soil Moisture and Soil Water Isotopes at the Broadleaf Forest Site

Figure 43 shows the 25-year baseline simulations of soil moisture and soil water isotopes dynamics at the broadleaf forest site at a daily time step as an example. In general, the model effectively captures the magnitude, variabilityfrequency, extremes, and timing of soil moisture dynamics. Model results show sSurface soil moisture shows higher variability than deeper layers. Based on the Kling-Gupta Efficiency (KGE), soil moisture simulations generally appear to perform better in the deep layer than in the shallow and lower layers, though this may partly reflect the more limited variance in deeper soil moisture. In addition, the model slightly overestimates low soil moisture in the deeper layers during wet summers (e.g., 2023, 2024) and underestimates soil moisture during dry winters (e.g., 2021 and 2022). Furthermore, sSoil water isotope simulations also perform well, with better performancehigher KGE values in the intermediate layer than in surface and deeper layers in terms of KGE. The uncertainty range of soil water isotope simulations is narrower than that of soil moisture, indicating lower uncertainty in the isotope predictions.

Formatted: English (United States)

Table 3 shows the Kling-Gupta Efficiency (KGE) and Root Mean Square Error (RMSE) values for soil moisture and soil water isotopes across different land use plots. In all other cases the KGEs for soil moisture are similar to

the broadleaved plot, and soil water isotopes are reasonably reproduced, indicating the model's robustness and transferability. These results provide strong support for the appropriateness of applying EcoPlot-iso to assess the impacts of alternative forest management scenarios in subsequent analyses. In addition, simulated evapotranspiration was independently evaluated against MODIS-derived ET for all land use types, with model performance quantified using RMSE and KGE metrics (Table S4). This independent evaluation provides further support for the model's ability to reproduce key water fluxes beyond the variables used for calibration.

Table 3. ~~Kling-Gupta Efficiency (KGE) values for soil moisture and δ^2H.~~ Model performance metrics for soil moisture and soil water isotopes (δ^2H) at each land use site over the full evaluation period (2000–2024), evaluated using the Kling–Gupta Efficiency (KGE) and the root mean square error (RMSE, mm for soil moisture and ‰ for δ^2H). Metrics are computed by comparing observed and simulated time series at each soil depth. ~~based on observed values compared to the mean simulated values.~~

~~Forest sites~~	~~Soil moisture~~			~~Soil water isotope δ^2H~~		
	~~Upper soil compartment~~	~~Lower soil compartment~~	~~Deep soil compartment~~	~~Upper soil compartment~~	~~Lower soil compartment~~	~~Deep soil compartment~~
~~Broadleaf Forest~~	~~0.60~~	~~0.72~~	~~0.84~~	~~0.58~~	~~0.74~~	~~0.64~~
~~Agroforestry~~	~~0.72~~	~~0.76~~	~~0.78~~	~~0.81~~	~~0.84~~	~~0.78~~
~~Grassland~~	~~0.87~~	~~0.67~~	~~0.71~~	~~0.72~~	~~0.76~~	~~0.60~~
~~Cropland~~	~~0.53~~	~~0.54~~	~~0.71~~	~~0.82~~	~~0.84~~	~~0.28~~

Sites	Soil moisture						Soil water isotope (δ^2H)					
	Upper		Lower		Deep		Upper		Lower		Deep	
	KGE	RMSE	KGE	RMSE	KGE	RMSE	KGE	RMSE	KGE	RMSE	KGE	RMSE
Broadleaf Forest	~~0.56~~	~~5.8374~~	~~0.75~~	~~7.51~~	~~0.84~~	~~13.32~~	~~0.58~~	~~13.23~~	~~0.74~~	~~8.35~~	~~0.68~~	~~8.43~~
Conifer forest	0.610	5.777.97	0.685	8.68	0.7069	5.56	0.679	11.69	0.802	6.94	0.504	13.09
Agroforestry	0.72	5.22	0.79	6.63	0.778	23.43	0.823	8.09	0.853	10.45	0.798	8.98
Grassland	0.89	1.67	0.710	6.18	0.724	16.01	0.713	9.07	0.775	7.69	0.61	8.36
Cropland	0.53	5.84	0.623	8.88	0.71	22.36	0.834	8.36	0.854	9.19	0.365	13.71

Formatted ... [74]
Formatted ... [75]
Formatted ... [76]
Formatted ... [77]
Formatted ... [78]
Formatted ... [79]
Formatted ... [80]
Formatted ... [81]
Formatted ... [82]
Formatted ... [83]
Formatted ... [84]
Formatted ... [85]
Formatted ... [86]
Formatted ... [87]
Formatted ... [88]
Formatted ... [89]
Formatted ... [90]
Formatted ... [91]
Formatted ... [92]
Formatted ... [93]
Formatted ... [94]
Formatted ... [95]
Formatted ... [96]
Formatted ... [97]
Formatted ... [98]
Formatted ... [99]
Formatted ... [100]
Formatted ... [101]
Formatted ... [102]
Formatted ... [103]
Formatted ... [104]
Formatted ... [105]
Formatted ... [106]
Formatted ... [107]
Formatted ... [108]
Formatted ... [109]
Formatted ... [110]
Formatted ... [111]
Formatted ... [112]
Formatted ... [113]
Formatted ... [114]
Formatted ... [115]
Formatted ... [116]
Formatted ... [117]
Formatted ... [118]

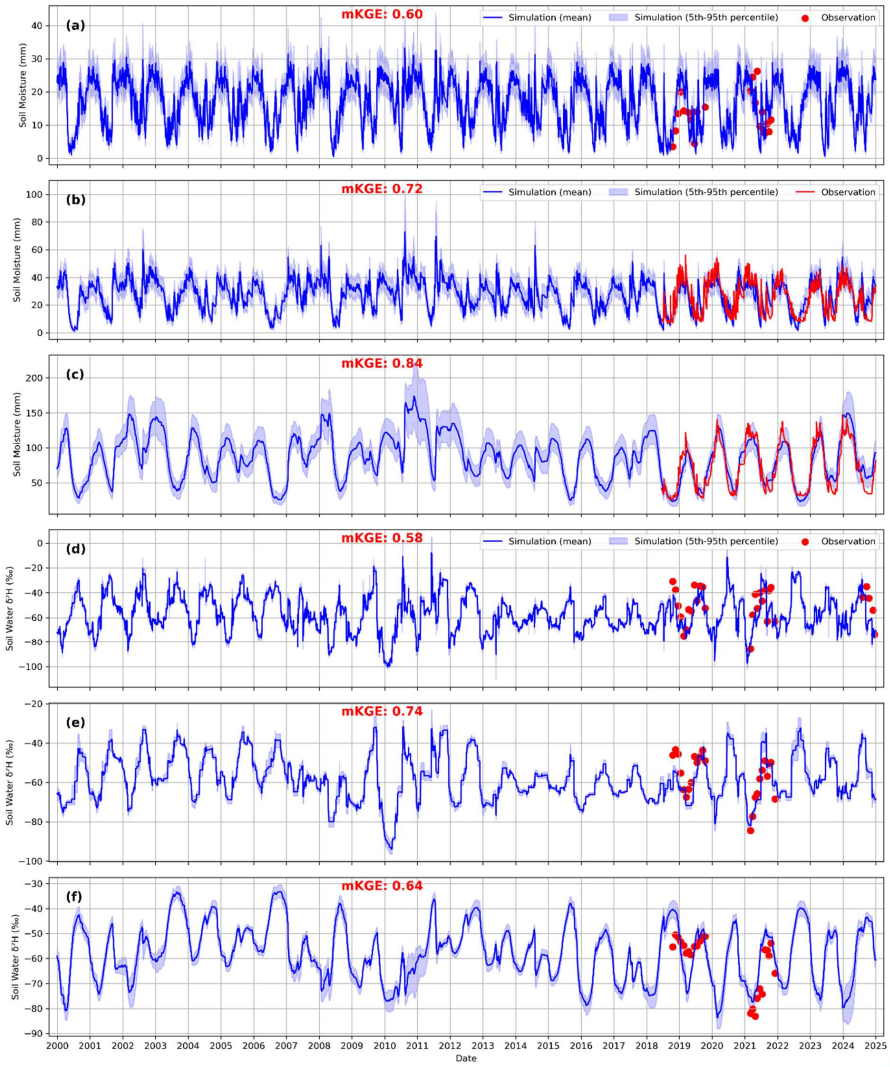
(a)
mKGE: 0.60
Simulation (mean)
Simulation (5th-95th percentile)
Observation
Soil Moisture (mm)
(b)
mKGE: 0.72
(c)
mKGE: 0.84
(d)
mKGE: 0.58
Soil Water δ²H (‰)
(e)
mKGE: 0.74
(f)
mKGE: 0.64
Date

492

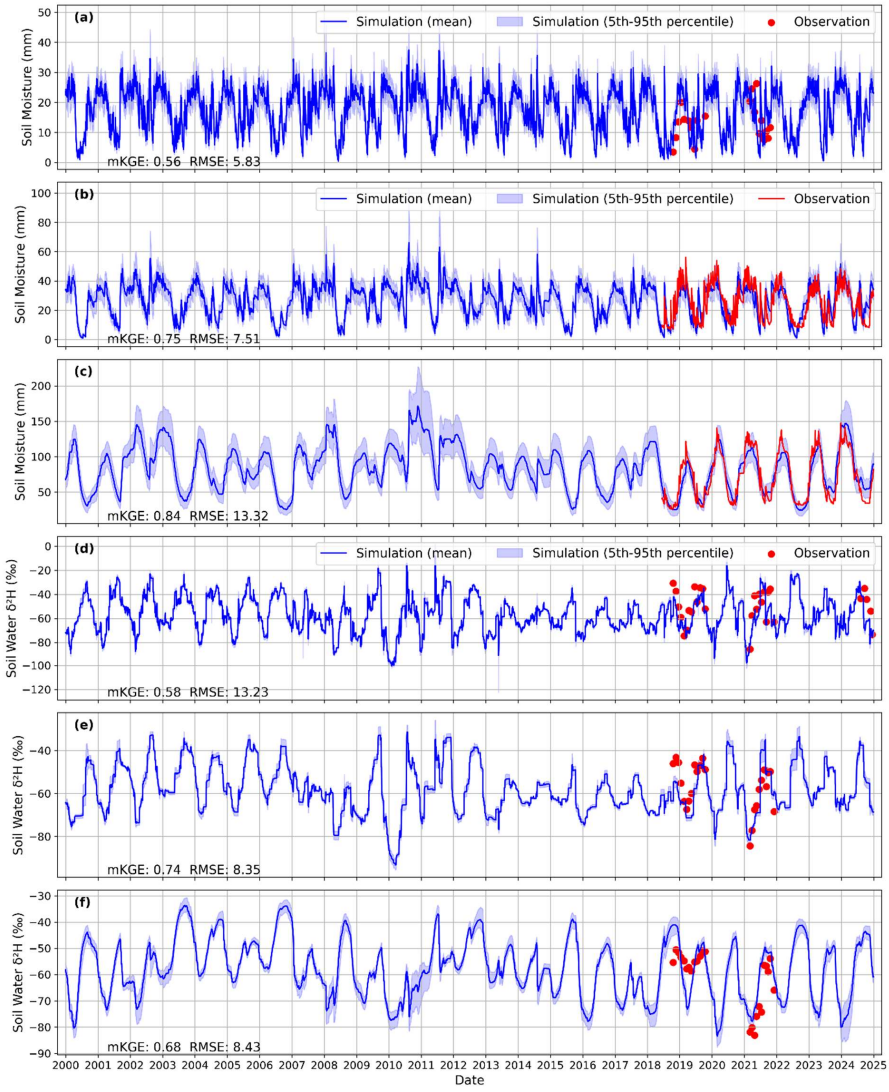

Figure 43. Long-term (2000–2024) simulations of soil moisture and soil water isotope (δ^2H) at three different depths using EcoPlot-iso at a broadleaf forest site in the Demnitzer Millcreek catchment. (a–c) Simulated (mean ± 5th–95th percentile) and observed soil moisture at surface (0–10 cm), lower (20–30 cm), and deeper (30–100 cm) layers. (d–f) Simulated (mean ± 5th–95th percentile) and observed soil water isotopic composition (δ^2H) at corresponding depths. The blue line represents the mean value of the 100 best simulations, while the shaded area indicates the range between the 5th and 95th percentiles of these simulations. The red points and red line represent observed values. Kling-Gupta Efficiency (KGE) values for each simulation are indicated in the respective panels.

Formatted: Line spacing: single

4.2 Water Balance Components Under Different Wetness Conditions at the Broadleaf Forest Site

Figure 45 presents the mean monthly water balance components and their changes between dry and wet years for the baseline simulation at the broadleaved forest site from 2000 to 2024. Groundwater recharge dominates blue water fluxes, while surface runoff is rare and occurs only during extreme summer rainfall events (Fig.~~ure~~ 54a). Transpiration and canopy evaporation dominate in summer, while soil evaporation peaks in spring. Across dry and wet years, groundwater recharge shows the strongest sensitivity to interannual wetness, with reduced recharge during dry years and enhanced recharge during wet years following precipitation anomalies (Figs. 5b and S1).~~In dry years, recharge declines and dominates the intermonthly variation (Figure 4b), whereas in wet years, it increases following precipitation anomalies (Figure 4c).~~ In contrast, transpiration remains relatively stable despite differences in annual wetness, indicating resilient vegetation function. ~~Despite differences in annual wetness—across both dry and wet years—transpiration remains relatively stable (Figure 4d), indicating resilient vegetation function.~~ This stability likely reflects the mature age of the forest (~60 years), although gradual changes in forest structure over the 20-year period may also play a role. Corresponding water balance results for the conifer forest and agroforestry sites are provided in the Supplementary Material (Fig. S9). Across the three forest types, the conifer forest exhibits the largest changes in groundwater recharge between dry and wet years, particularly in August, whereas agroforestry shows comparatively smaller changes than the broadleaf forest, indicating higher ecohydrological resilience. Overall, ~~T~~these seasonal patterns offer key insights into water partitioning under ~~broadleaf~~ three forest baseline conditions and establish an important baseline for evaluating the impacts of alternative forest management scenarios.

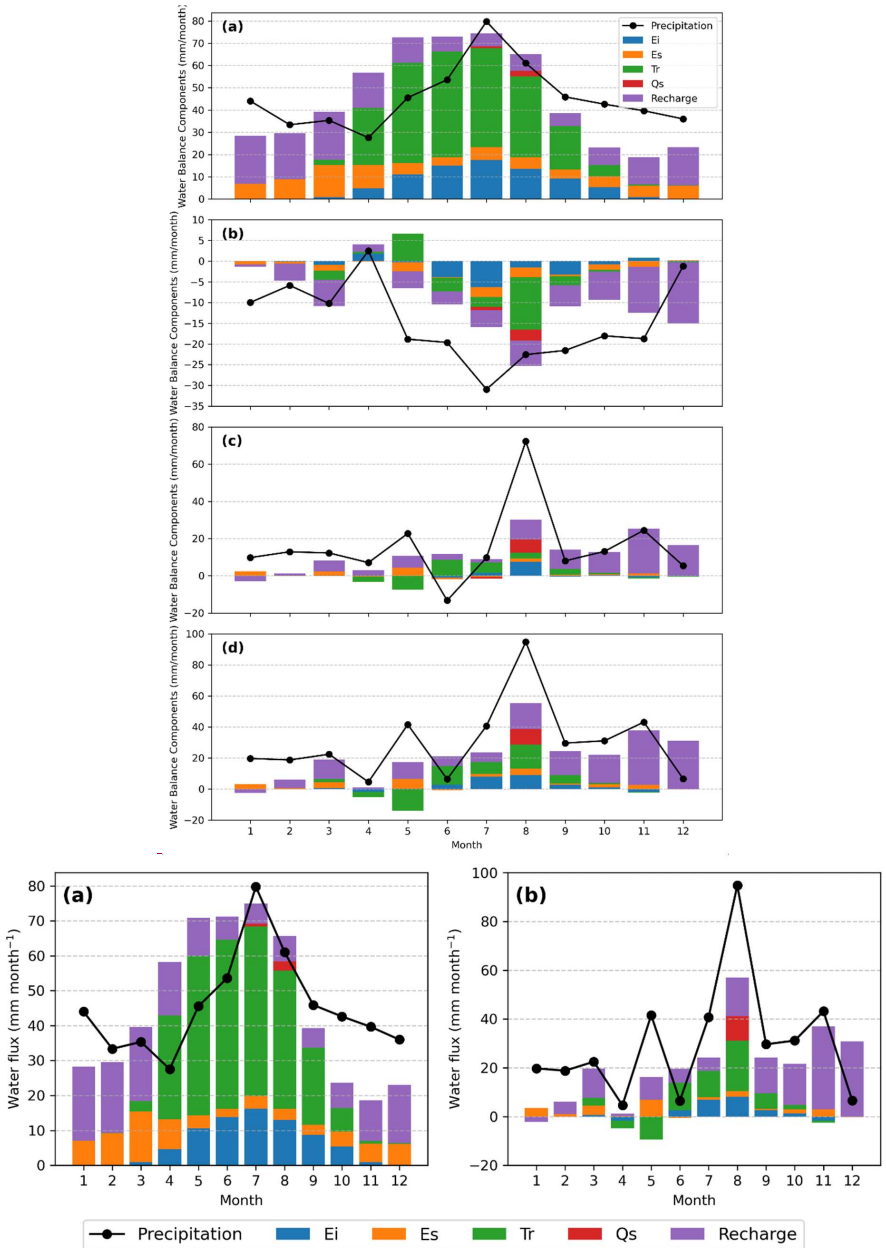

Figure 54. Mean monthly water balance components ~~for the period 2000–2024, simulated using EcoPlot-iso~~ for the broadleaf forest site in the Demnitzer Millcreek catchment over 2000–2024, simulated with EcoPlot-iso using ~~, based on~~ the mean of the best 100 parameter sets (see Section 3.4 for details). Stacked bars show monthly totals of interception evaporation (Ei), soil evaporation (Es), transpiration (Tr), surface runoff (Qs), and groundwater recharge, while the black line indicates precipitation (P). (a) Long-term mean monthly water balance

(mm month^{-1}). ~~(b) Deviations of dry years (2006, 2018, 2022) from the long-term mean. (c) Deviations of wet years (2002, 2007, 2010, 2023) from the long-term mean.~~ (~~b~~d) Differences between wet years (2002, 2007, 2010, 2023) and dry years (2006, 2018, 2022), expressed as wet minus dry (mm month^{-1}).~~.~~

4.3 Impacts of Forest Management on Water Partitioning and Soil Moisture

Results in this section are based on the full forest management scenario framework, including all nine forest–site Scenario Groups and their associated ensemble simulations (Fig. 3), rather than on the observed baseline configurations alone.

4.3.1 Water Balance and Partitioning Across Forest Types

Figure ~~5~~6 compares the mean annual water balance components ~~simulated~~ across broadleaf forest, coniferous forest, and agroforestry types based on the ~~average~~ ensemble mean of ~~the best 100~~ simulations derived from the paired vegetation–site soil parameter configurations (Fig. 3), under reference canopy and rooting conditions (LAI scaling = 1; $\beta = 1 \times \beta$). ~~. LAI was derived from DMC data for each forest type, while the LAI scaling factor and root parameters were kept constant across vegetation types.~~ Results showed that evapotranspiration under coniferous forests accounted for 78% more of annual precipitation than broadleaf~~ved~~ forest~~s~~, and ~~13~~11% more than in agroforestry systems. This was primarily due to higher transpiration (Tr) and canopy interception evaporation (Ei). In contrast, soil evaporation (Es) and groundwater recharge (Recharge) were lowest in conifers and highest in agroforestry. Agroforestry had 11~~13~~% more groundwater recharge relative to annual precipitation than conifers, and 44% more than broadleaf forests. Across forest types, the largest fraction of transpiration originated from the upper soil layer (Tr_Upper), reflecting its closer coupling to precipitation inputs and higher soil moisture availability.~~Transpiration partitioning across root zones (Tr_Upper, Tr_Lower, Tr_Deep) was similar across all forest types,~~ while surface runoff (Qs) remained minimal and nearly identical. These results reflect the influence of forest structure and canopy cover on ecohydrological partitioning, with coniferous systems favoring atmospheric losses and agroforestry promoting soil evaporation and subsurface recharge. They underscore the trade-offs between evapotranspiration and groundwater recharge across different forest types.

Formatted: Superscript

Formatted: Font: Not Bold, English (United States)

Formatted: Font: Not Bold, English (United States)

Formatted: Font: Not Bold, English (United States)

Formatted: None, Space Before: 0 pt, After: 6 pt, Line spacing: 1.5 lines, Don't keep with next, Don't snap to grid

Formatted: Font: Italic

Formatted: Font: Italic

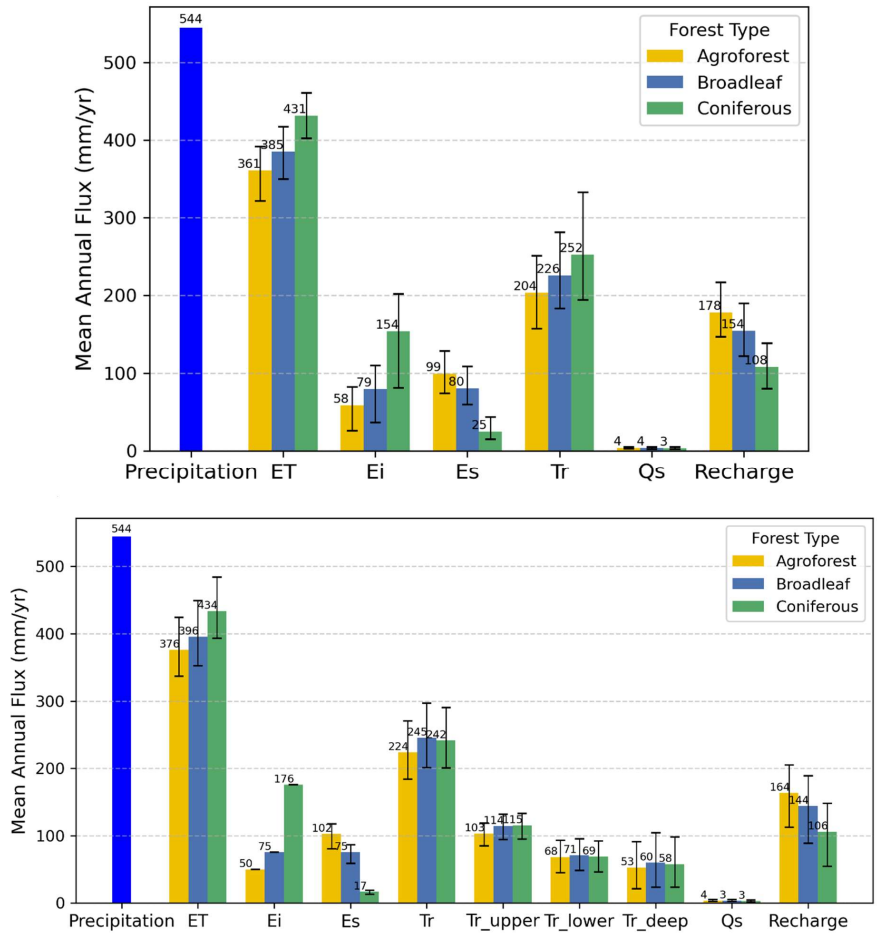

Figure 65. Comparison of mean annual water balance components across different forest types: broadleaf (blue), coniferous (green), and agroforestry (yellow). Bars represent the mean annual flux based on 25-year totals, with error bars indicating the 5th and 95th percentile ranges of the 100 best simulations. All simulations were conducted under baseline conditions with a fixed forest root parameter β of 0 and LAI scaling factor of 1.0.

Figure 76 presents ternary diagrams illustrating the relative partitioning of key water flux components across three forest types ~~under~~ based on individual simulations from the paired vegetation–site soil parameter configurations under reference canopy and rooting conditions~~baseline conditions~~. ~~This shows the predominance in t~~Transpiration predominates in all three forest types ~~eases~~ (Fig. 76a). The ~~C~~conifer~~rous~~ forest~~s~~ exhibit ~~show~~ a distinct pattern, characterized by ~~with~~ the lowest soil evaporation (Es) ~~(Fig. 6a)~~ and the highest interception evaporation (Ei) partitioning ~~groundwater recharge (Fig. 6b)~~ compared to broadleaf forest and agroforestry ~~systems~~ systems (Fig. 7a). In terms of green–blue water partitioning, the agroforestry system shows the largest groundwater recharge contribution (Fig. 7b). Broadleaf and agroforestry forests display largely overlapping partitioning patterns overall, although interception evaporation and total evaporation differ notably between the two (Fig. 7a–b). ~~In contrast,~~

~~broadleaf and agroforestry forests display largely overlapping partitioning patterns, except for soil evaporation, which differs notably between the two.~~Differences in soil properties also influence transpiration partitioning, following the order agroforestry site > broadleaf site > conifer site. The conifer site is characterized by coarse sandy soil with lower water retention and faster drainage, whereas the agroforestry site has greater water-holding capacity, which likely contributes to the observed differences in transpiration.

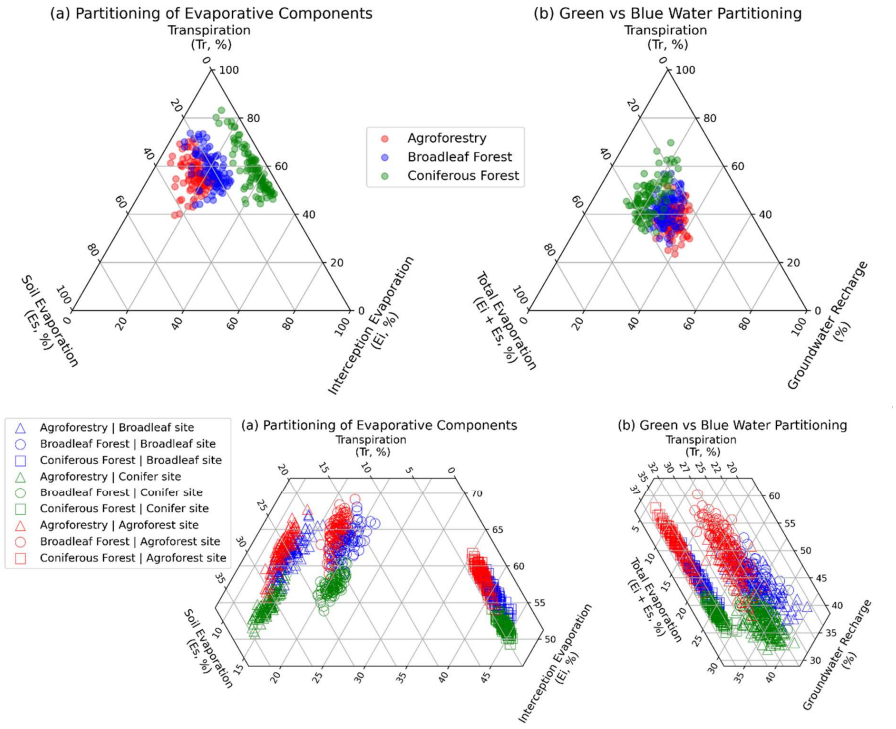

Figure 76. Water flux partitioning illustrated using ternary diagrams based on individual model simulations derived from the paired vegetation–site soil parameter configurations for three forest types: agroforestry, broadleaf forest, and coniferous forest, under reference canopy and rooting conditions (LAI scaling = 1.0; β = 1 × β). ~~Water flux partitioning illustrated using ternary plots based on 100 model simulations for three forest types: Agroforestry, Broadleaf Forest, and Coniferous Forest, under baseline conditions (root parameter β = 0, LAI scaling factor = 1.0).~~ (a) Partitioning of total evapotranspiration into transpiration (Tr), soil evaporation (Es), and interception evaporation (Ei). (b) Partitioning of water fluxes into green water (Tr and E = Ei + Es) and blue water (groundwater recharge). Each point represents the normalized annual mean flux from a 25-year simulation. Colored markers denote different forest types.

4.3.2 ~~I~~Annual Mean Water Flux Responses to Forest Management Scenarios~~nterannual Patterns and Variability of Water Fluxes~~

The annual mean responses of key ecohydrological fluxes to forest management scenarios across all paired vegetation–site configurations are summarized in Figure 8, while the detailed number and visualization of green and blue water partitioning are provided in the Figure S10 in Supplementary Material. Figure S~~7~~10 presents

Formatted: Font color: Auto

Formatted: Font: Not Bold

Formatted: Font: Not Bold, Italic

Formatted: Font: Not Bold

Formatted: Font: Not Bold, Italic

Formatted: Font: Not Bold

~~provides a detailed visualization of the isotope-informed green and blue water partitioning across different forest management scenarios. The~~ heatmaps ~~present~~ of ~~the key ecohydrological fluxes, including~~ evapotranspiration (ET) ~~(a–c)~~, groundwater recharge (Recharge) ~~(d–f)~~, transpiration (Tr) ~~(g–i)~~, ET partitioning (ET/P) ~~(j–l)~~, groundwater recharge partitioning (Recharge/P) ~~(m–o)~~ and green water partitioning (Tr/ET) ~~(p–r)~~ for ~~the three forest types:~~ agroforests, broadleaf forest~~s~~, and coniferous forest~~s~~ scenarios.

Across all forest management scenarios, annual mean ~~E~~evapotranspiration ~~(ET)~~ ranges from 2853~~1~~ mm/yr to 4534 mm/yr ~~across different scenarios~~, with ET ~~proportion~~ fraction relative to precipitation varying ~~from~~ between 0.~~42~~ 52 ~~to~~ and 0.8~~4~~ 3(Fig. S10)~~, respectively~~. In contrast, groundwater recharge ranges from ~~88~~ 85 mm/yr to ~~307~~ 254 mm/yr~~.~~, reflecting strong sensitivity to vegetation structure and canopy density. Annul mean t~~T~~ranspiration (Tr) varies between ~~49~~ 77 mm/yr and ~~238~~ 261 mm/yr, with the corresponding green water partitioning (Tr/ET) ranging from 0.~~21~~ 27 to 0.~~53~~64. These results underscore the significant influence of vegetation type and structure on ecohydrological fluxes and water partitioning outcomes.

Consistent with these detailed patterns, Figure 8 shows that ~~Furthermore, annual mean values show that~~ both transpiration and evapotranspiration increase with higher LAI scaling factors, while groundwater recharge decreases ~~(Figure 8)~~. Figures 8a and 8b illustrate the trade-off between increased ET and reduced groundwater recharge under different forest management scenarios. Transpiration and ET rise rapidly at first, then slow down and transpiration even slightly decreases for conifer forests due to soil moisture limitation (Fig~~ure~~ 8c). This decline is not observed in broadleaf or agroforestry systems, likely due to their different seasonal LAI patterns. While summer LAI values for broadleaf and coniferous forests may be similar, the consistently high year-round LAI in conifers can exacerbate moisture stress.

At higher LAI levels, transpiration decreases slightly while canopy interception ~~and~~ evaporation ~~from the canopy~~ increase (Fig~~ure~~ S11~~4~~). In dense coniferous stands, excessive interception and persistently dry soils limit root water uptake, reducing vegetation function. This highlights a trade-off between transpiration and interception evaporation. The resulting moisture limitation suggests that such high-density forests may not be sustainable under water-limited conditions, as this negative feedback could constrain long-term forest growth and persistence. In addition, forests with shallow-rooted trees~~species~~—such as young stands ~~trees~~—tend to transpire less, generate more groundwater recharge, and exhibit lower Tr/ET ratios compared to deep-rooted forests. However, even at constant LAI, transpiration declines with increasing canopy density, suggesting that rooting depth alone cannot compensate for moisture limitations in dense forests.

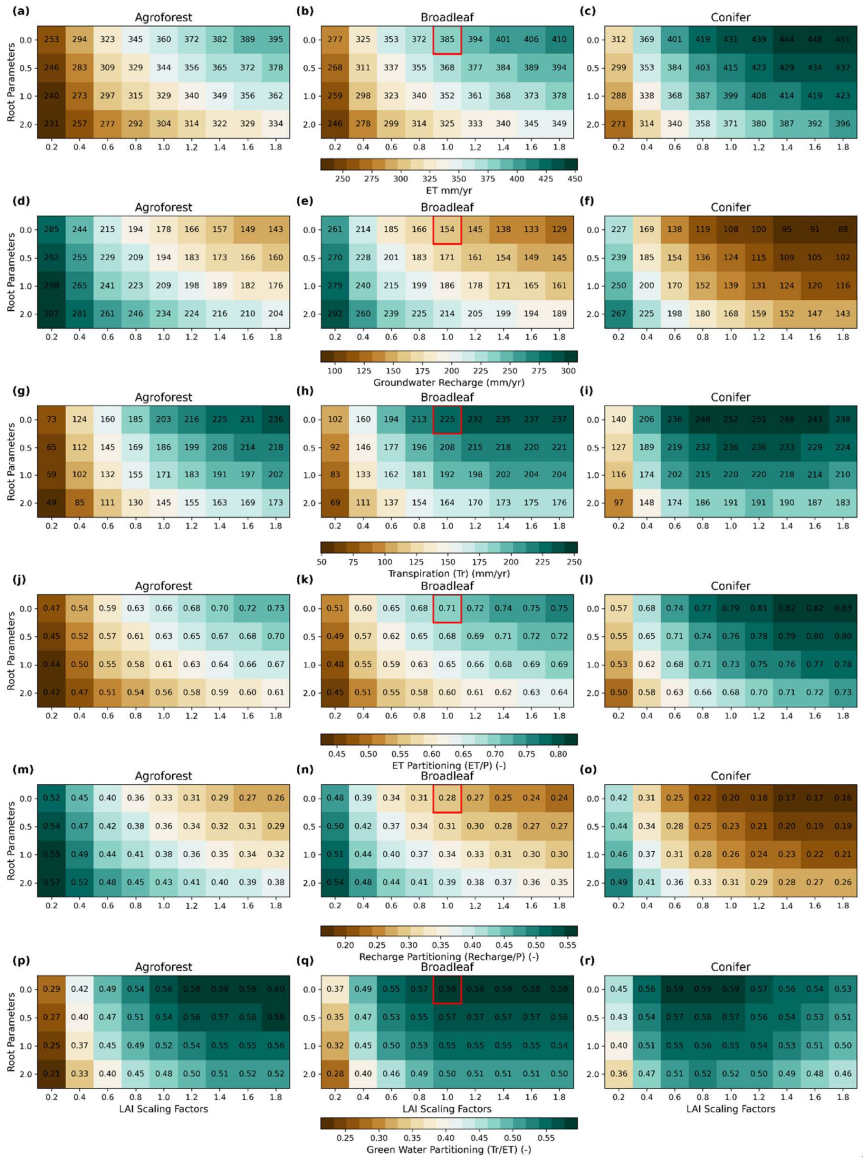

Figure 7. Green and blue water partitioning across forest types and LAI scaling factors. The heatmaps illustrate evapotranspiration (ET) (a–c), groundwater recharge (d–f), transpiration (Tr) (g–i), ET partitioning (ET/P) (j–l), and green water partitioning (Tr/ET) (m–o) for three forest types (Agroforest, Broadleaf, and Conifer). The x-axis represents scaling factors (forest density), while the y-axis represents root parameters (forest ages). Each heatmap includes numeric values for clarity, with red-outlined cells indicating the baseline simulations (Broadleaf forest, scaling factor = 1, root parameter = 0).

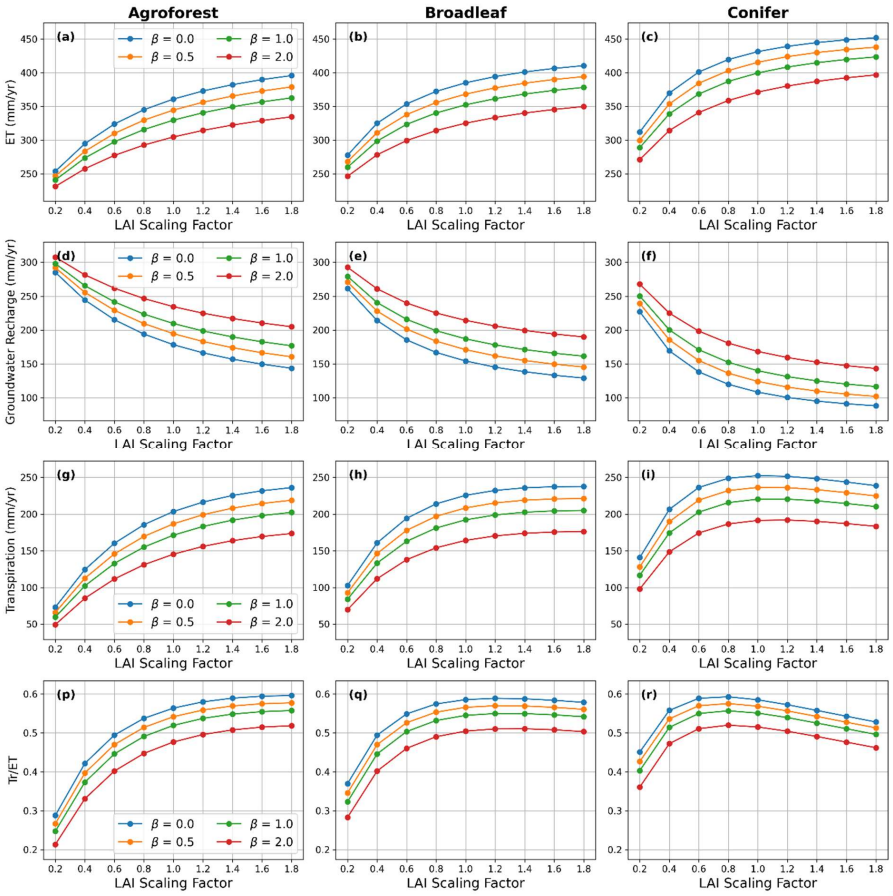
Agroforest
Broadleaf
Conifer
(a)
(b)
(c)
(d)
(e)
(f)
(g)
(h)
(i)
(p)
(q)
(r)
β = 0.0
β = 0.5
β = 1.0
β = 2.0
ET (mm/yr)
Groundwater Recharge (mm/yr)
Transpiration (mm/yr)
Tr/ET
LAI Scaling Factor

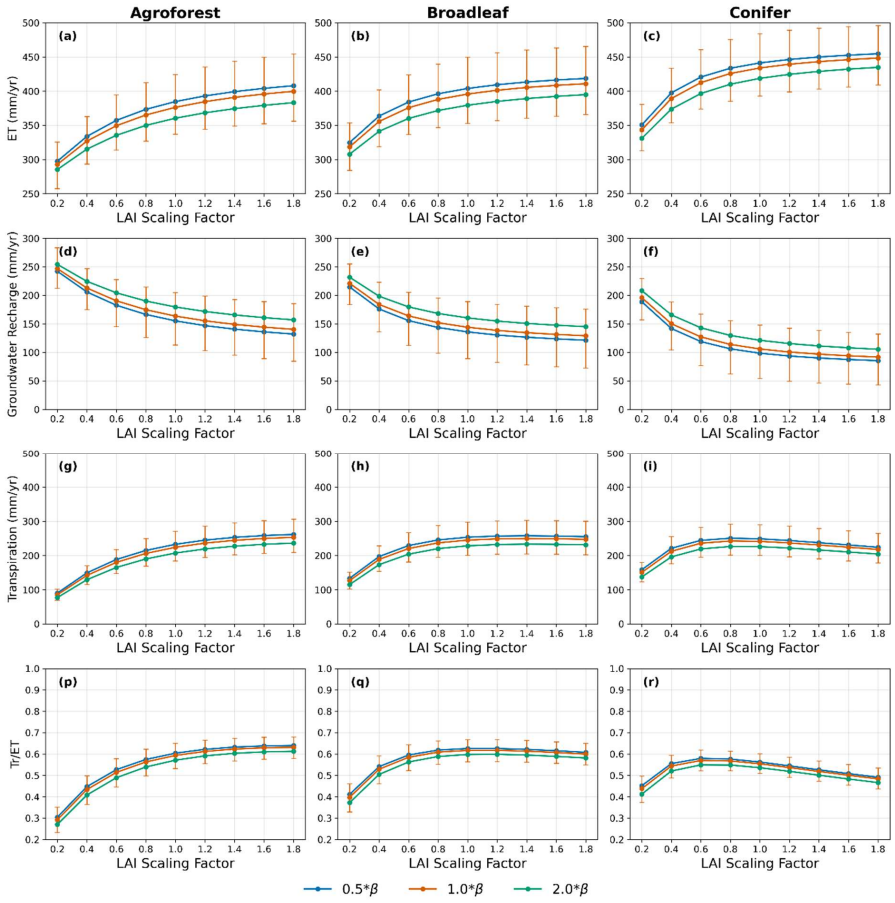

Figure 8. Annual mean ecohydrological fluxes for three forest types (Agroforest, Broadleaf, and Conifer) under varying LAI scaling factors and root depth scenarios~~.~~, based on the ensemble mean of simulations derived from the paired vegetation–site soil parameter configurations (Figure 3). Panels (a)–(c) show evapotranspiration (ET), (d)–(f) show groundwater recharge, (g)–(i) show transpiration, and (p)–(r) show the ratio of transpiration to total evapotranspiration (Tr/ET). Lines represent different rooting depth scenarios (β), while vertical bars denote the 5th–95th percentile range across ensemble simulations for the baseline rooting scenario (β = 1 × β).~~Each line represents a different forest age class (i.e., root depth) denoted by β values.~~

Formatted: Font: Italic

4.3.3 ~~Seasonal and~~ Monthly Dynamics of Water Fluxes Responses to Forest Management Scenarios

Figure 9 shows monthly deviations in water balance components ~~under~~ across~~different~~ forest management scenarios, based on the ensemble mean of simulations derived from the paired vegetation–site soil parameter configurations (Fig. 3) under reference canopy and rooting conditions (LAI scaling = 1; β = 1 × β)~~relative to a baseline broadleaf forest~~. Relative differences among forest types indicate that ~~A~~agroforestry ~~scenarios tend~~exhibit ~~to have~~ lower transpiration and canopy evaporation, but higher soil evaporation during summer

compared to broadleaf forests (Fig. 9a). They are also associated with greater groundwater recharge from summer through the following winter. A shift from broadleaf to conifer forests is expected to have a greater impact on the water balance than the shift from agroforest to broadleaf (Fig. 9a and 9b). Compared to broadleaf forests, conifer forests exhibit higher simulated transpiration in March (Fig. 9b), driven by increased potential evapotranspiration and a relatively higher leaf area index (LAI) under wet soil conditions. This difference diminishes as the LAI of broadleaf forests increases in spring.

Changes in the LAI scaling factor influence water balance components in summer, increasing transpiration and canopy evaporation while reducing recharge and soil evaporation (Fig. 9c and 9d). Increasing the LAI scaling factor from 0.4 to 1.0 has a greater impact than reducing it from 1.6 to 1.0, as vegetation water use responds more sensitively at low LAI values but plateaus at higher values due to energy or soil moisture limitations. Altering the forest root parameter (β), while using the same LAI time series, primarily affects deep-layer transpiration, reducing total transpiration and increasing recharge. Other water balance components remain unchanged because the LAI time series is held constant.

Figure 10 extends the monthly analysis by explicitly comparing water balance responses between wet and dry years across forest type, canopy density, and rooting scenarios. In contrast to Figure 9, which presents mean monthly deviations relative to reference conditions, Figure 10 highlights how these deviations differ under contrasting hydroclimatic conditions, thereby isolating drought-sensitivity effects.

For agroforestry relative to broadleaf forests, hydroclimatic contrasts primarily affect groundwater recharge and transpiration, with the largest wet–dry differences occurring in late summer ~~August~~ (Fig. 10a). This indicates a more buffered late-summer transpiration response in agroforestry systems under drought conditions. In contrast, differences between coniferous and broadleaf forests show the largest wet–dry contrasts in transpiration during May (Fig. 10b), rather than March as indicated by the mean monthly deviations in Figure 9b. This seasonal shift indicates that conifer transpiration is most drought-sensitive during the later spring period, likely reflecting sustained year-round transpiration and associated soil moisture drawdown in conifer forests, and highlighting differences in early growing-season water-use strategies between coniferous and broadleaf forests.

Figures 10c and 10d show that wet–dry differences are largest in summer (August), indicating that drought conditions amplify ecohydrological differences between low and high canopy density, as well as between shallow and deep root, particularly for transpiration and groundwater recharge. Overall, Figure 10 demonstrates that hydroclimatic extremes not only modify the magnitude of vegetation controls on water partitioning but also shift their seasonal expression, with important implications for ecohydrological resilience under future drought conditions.

Formatted: Font color: Text 1

~~Figure 10 illustrates the relative monthly deviations in evapotranspiration (ET) and groundwater recharge under varying forest types, LAI scaling factors, and root distributions, relative to a baseline broadleaf forest. Agroforestry increases recharge during the low-flow season (June–December) (Fig. 10a), while conifer forests consistently reduce recharge and exhibit substantially higher ET in winter (Fig. 10b). The effects of LAI scaling are most pronounced during the low-flow season. A higher LAI (scaling factor = 1.6) increases ET and reduces recharge, whereas a lower LAI (scaling factor = 0.4) has the opposite effect. However, at higher LAI values, the~~

~~magnitude of relative deviation diminishes, suggesting a saturation effect. Root distribution also affects seasonal water balance. Scenarios with deeper roots tend to reduce recharge, while shallow root systems enhance recharge during dry months across all forest types. Overall, these results highlight the sensitivity of summer water balance to vegetation structure. Agroforestry consistently exhibits more ecohydrologically resilient responses than conifer forests, particularly under drought-sensitive conditions.~~

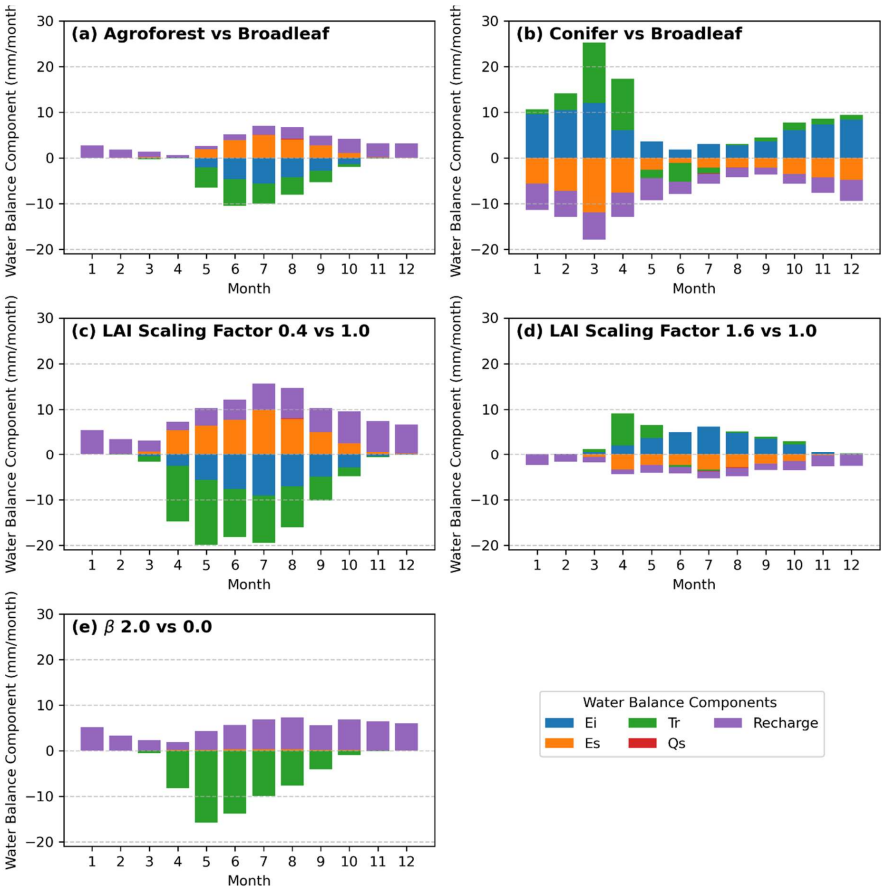
(a) Agroforest vs Broadleaf
(b) Conifer vs Broadleaf
(c) LAI Scaling Factor 0.4 vs 1.0
(d) LAI Scaling Factor 1.6 vs 1.0
(e) β 2.0 vs 0.0
Water Balance Component (mm/month)
Month
Water Balance Components
Ei
Es
Tr
Qs
Recharge

690

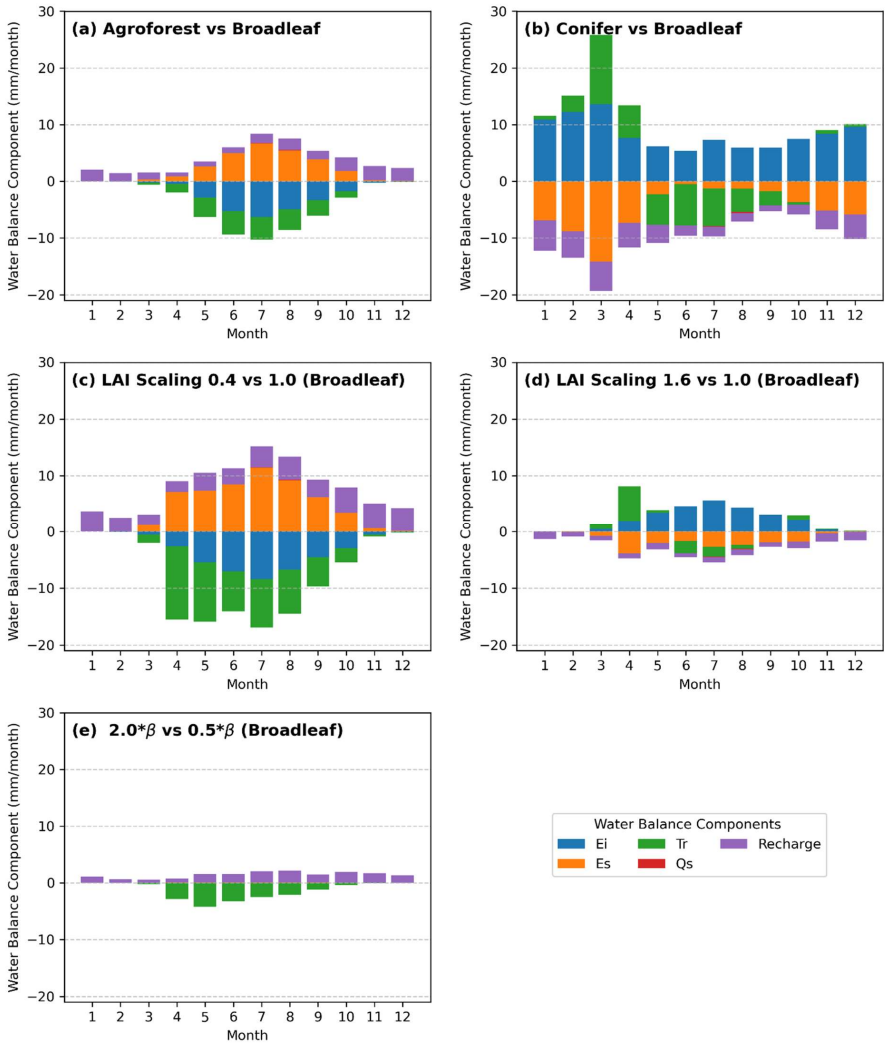

Figure 9. Monthly deviations of water balance components relative to the baseline broadleaf forest scenario~~.~~, based on the ensemble mean of simulations derived from the paired vegetation–site soil parameter configurations (Fig. 3) under reference canopy and rooting conditions (LAI scaling = 1; β = 1 × β).Each panel illustrates the deviation of monthly water balance components from the baseline simulation, with only one parameter modified in each scenario: (a) Agroforest, (b) Conifer forest, (c) LAI scaling factor = 0.4, (d) LAI scaling factor = 1.6, and (e) Root parameter β = 2.0. Tr: transpiration, Ei: canopy evaporation, Es: soil evaporation, Qs: surface runoff, Recharge: groundwater recharge.

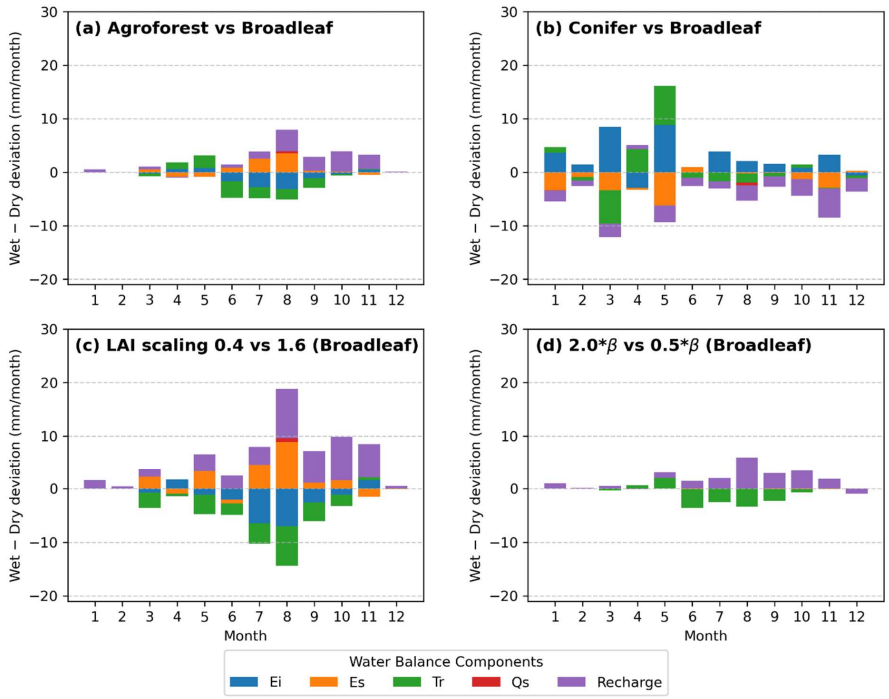

Figure 10. Monthly differences in water balance component deviations between wet and dry years across forest type, LAI scaling, and rooting (β) scenarios. For each panel, values show the difference between wet-year and dry-year deviations of a given scenario relative to its reference scenario; positive (negative) values indicate stronger (weaker) contributions during wet years. Panels show: (a) Agroforest vs. Broadleaf; (b) Conifer vs. Broadleaf; (c) *LAI* scaling 0.4 vs. 1.6 for Broadleaf; (e) 2.0 × β vs. 0.5 × β for Broadleaf. Stacked bars indicate contributions from interception evaporation (*Ei*), soil evaporation (*Es*), transpiration (*Tr*), surface runoff (*Qs*), and groundwater recharge (Recharge). Wet years are 2002, 2007, 2010, and 2023; dry years are 2006, 2018, and 2022.

Formatted: Font: Bold

Formatted: Space Before: Auto, After: Auto, Don't snap to grid

Formatted: Font: Italic

Formatted: Font: Italic

Formatted: Font: Italic

Formatted: Font: Italic

Formatted: Font: Italic

Formatted: Font: Italic

Formatted: Font: Italic

Formatted: Font: Italic

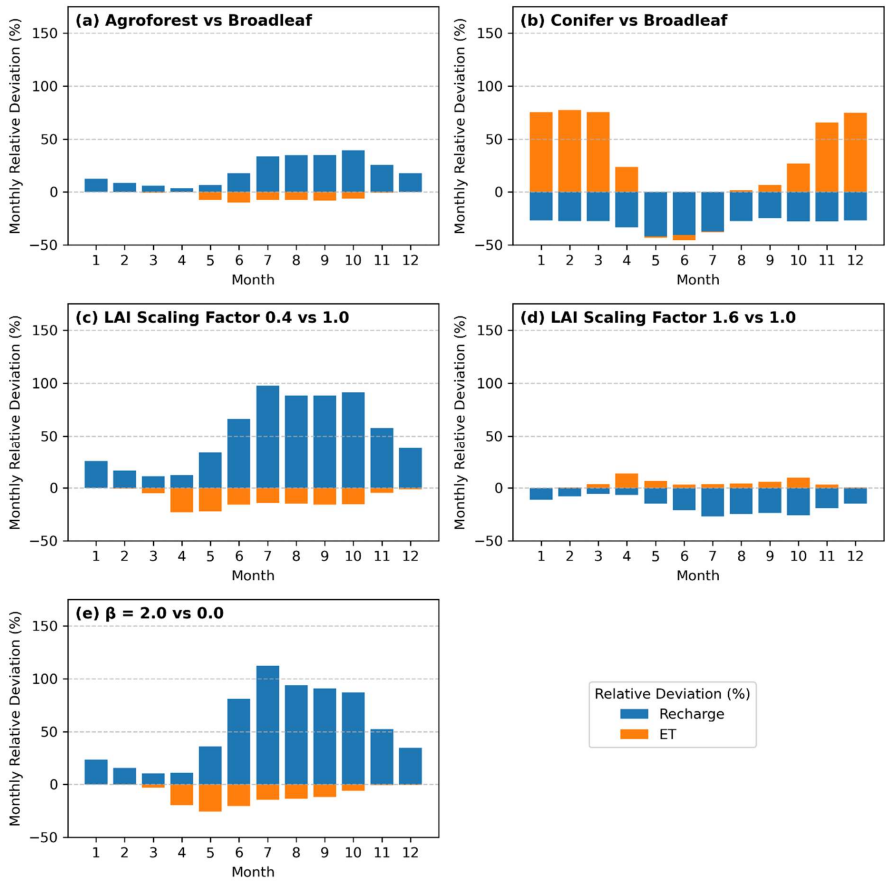

~~**Figure 10.** Monthly relative deviations in evapotranspiration (ET) and groundwater recharge, calculated as (scenario − basedline)/baslinline) ×100%, relative to the baseline broadleaf forest simulation. Each panel represents a different scenario in which one variable is modified while others are held constant: (a) Agroforest vs Broadleaf, (b) Conifer vs Broadleaf, (c) LAI scaling 0.4 vs 1.0, (d) LAI scaling 1.6 vs 1.0, and (e) Root parameter $\beta = 2.0$ vs 0.0.~~

4.3.4 Soil Moisture Anomalies

Figure 11 shows the relative summer soil moisture anomalies across three forest types and three soil layers. Anomalies are calculated as the percentage deviation from the long-term seasonal mean, enabling normalized comparison across forest types and soil layers. Conifer forests exhibit the strongest soil moisture anomalies, followed by broadleaf forests, while agroforests exhibit the least variability, indicating greater stability in soil moisture. Furthermore, among the three soil layers, the intermediate layer (10–30 cm) consistently shows stronger anomalies across all forest types, with magnitudes nearly double those of the other layers, highlighting its vulnerability during summer drought. In contrast, the surface layer (0–10 cm) and deep layer (30–100 cm) exhibit weaker anomalies, likely due to frequent soil moisture replenishment by summer rainfall in the surface layer and either more stable moisture retention or greater water storage capacity at depth that compensates for drought

impacts. Negative soil moisture anomalies are more pronounced in summer than in spring, reflecting the stronger seasonal drought effects and fluctuations in soil moisture (see Fig.~~ure~~ S12~~5 in the Supplementary Material~~). During spring, broadleaf forests and agroforests display similar negative soil moisture anomalies, suggesting comparable seasonal soil moisture dynamics between these forest types~~ (Figure S5)~~.

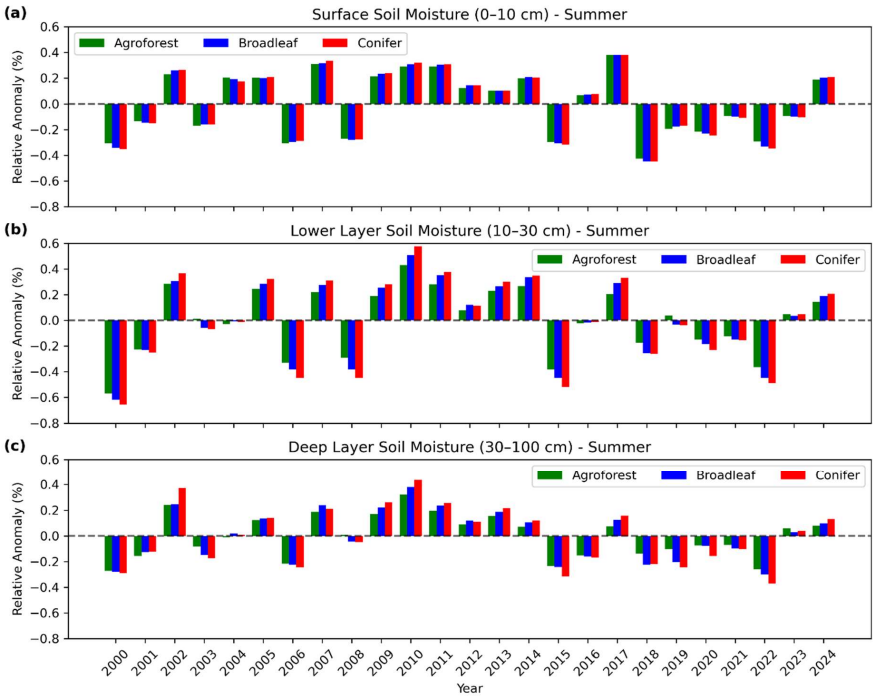
(a)
Surface Soil Moisture (0–10 cm) - Summer
Agroforest
Broadleaf
Conifer
Relative Anomaly (%)
(b)
Lower Layer Soil Moisture (10–30 cm) - Summer
(c)
Deep Layer Soil Moisture (30–100 cm) - Summer
Year

729

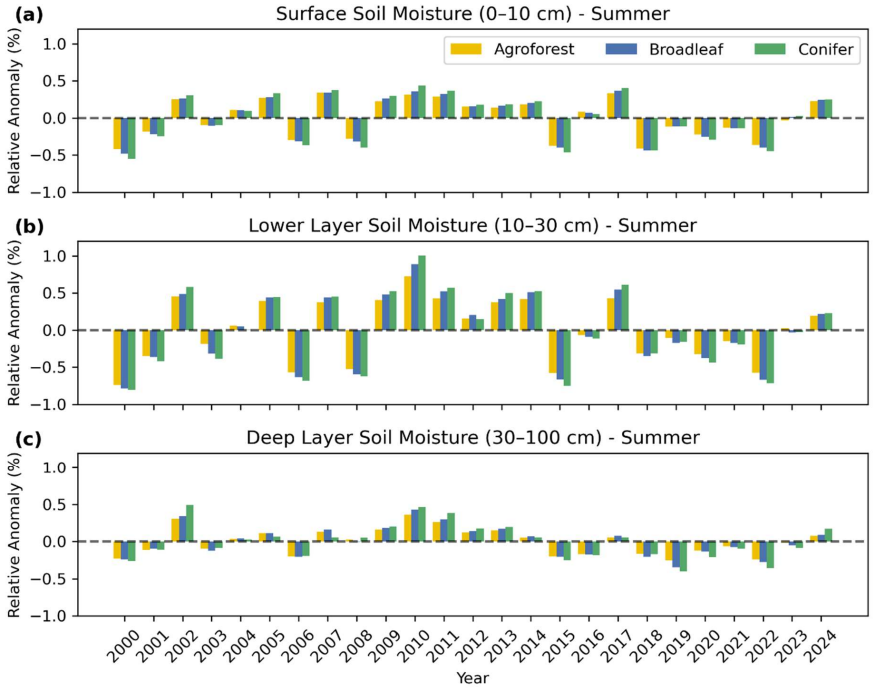

Figure 1~~1~~1. Relative summer (June–August) soil moisture anomalies ~~for summer (June–August)~~ across three soil layers: (a) surface (0–10 cm), (b) lower layer (10–30 cm), and (c) deep layer (30–100 cm) for three forest types (Agroforest, Broadleaf, Conifer)~~.~~. Results are based on the ensemble mean of simulations derived from the paired vegetation–site soil parameter configurations (Fig. 3) under reference canopy and rooting conditions (LAI scaling = 1; β = 1 × β). Bars represent deviations from the long-term mean, with positive values indicating wetter conditions and negative values indicating drier conditions.

5 Discussion

5.1 Vegetation Controls on Water Partitioning ~~and Ecohydrological Resilience~~ under Contrasting Forest Management Scenarios~~Implications of Forest Management Scenarios for Water Availability and Water Resource Management~~

Assessing the influence of different land use types on water availability is inherently challenging ~~due to~~because of the complex interactions among vegetation, climate, and soil properties (te Wierik et al., 2021; Zhang et al., 2001). Different vegetation types have distinct water demands, and their contrasting canopy structures affect how precipitation is intercepted~~,~~ and partitioned into infiltration, runoff, groundwater recharge, and evapotranspiration (Brauman et al., 2010). Vegetation management practices can substantially ~~significantly~~ alter these processes. Moreover, the effects of vegetation and canopy structure may vary depending on underlying soil characteristics (Geris et al., 2015). This complexity poses a significant challenge for land managers and policymakers, ~~especially~~ particularly in drought-sensitive regions ~~facing~~ experiencing increasing aridity under~~due to~~ climate change (Orth & Destouni, 2018). In such contexts, providing informed guidance on sustainable land cover choices is

Formatted: German (Germany)

increasingly important ~~to~~ for maintaining long-term water availability (Estrela & Vargas, 2012). In regions where forestry has traditionally been ~~an~~ a ~~important~~ dominant land use, shifting hydroclimatic conditions underscore the need to assess the resilience of different forest types and management practices (Quandt et al., 2023). This requires evaluating water yield across multiple temporal scales, including ~~how~~ the effects of forest management on ~~affects~~ annual and ~~seasonal~~ monthly water partitioning, and ~~its~~ their implications for residual water availability—specifically streamflow generation and groundwater recharge during low-flow periods (Brown et al., 2005; Neill et al., 2021).

Although complex, process-based ecohydrological models such as RHESSys and EcH$_2$O ~~can~~ are well suited to capturing ~~e~~ detailed interactions among hydrological processes and water fluxes in data-rich research settings, their broader application in forest and land management is often constrained ~~limited~~ by the ~~high~~ availability of observation data require~~ed~~~~ments~~ for model forcing and calibration, as well as ~~computational demand~~ (Fatichi et al., 2012; Kuppel et al., 2018; Tague & Band, 2004). In this study, we therefore adopt a parsimonious, tracer-aided, conceptual process-based modelling approach. This was ~~not~~ not to replace more complex models, but to provide robust and management-relevant insights into the dominant vegetation-structural controls governing water partitioning under different forest management scenarios. ~~In this study, we sought to apply a parsimonious tracer-aided modelling approach to provide insights into the effects of different forest management scenarios on water partitioning and land use resilience~~ This focus is particularly relevant for ~~in~~ Brandenburg, northeastern Germany, where recent droughts have ~~shown~~ highlighted ~~that~~ the vulnerability of traditional forest management practices ~~focused~~ dominated~~on~~ by ~~coniferous plantations of~~ Scots pine ~~may not be sustainable~~plantations (Luo et al., 2024). By employing the tracer-aided ecohydrological model EcoPlot-iso, we ~~used~~ developed and applied a generic ~~approach~~ framework to ~~help~~ quantify the long-term ~~impacts~~ effects of variations in forest type, ~~stand~~ forest density and root ~~depth~~ distribution on both blue and green water fluxes. The framework is based on idealized monoculture forest scenarios and ~~,~~ explicitly acknowledges that additional species-specific and process-level dynamics (e.g., stomatal regulation, VPD sensitivity, drought stress strategies) are not represent and remain important directions for future model development.~~.~~ While this study focused on idealized, homogeneous vegetation scenarios (broadleaf, conifer, and agroforestry) for clarity and comparability, EcoPlot-iso can be extended to simulate mixed-species stands, as its ecohydrological parameters are calibrated at the plot scale using a Monte Carlo approach, making it suitable for regions where diverse forest compositions are the norm. The applied LAI scaling range represents an intentionally broad, management-relevant envelope for exploring canopy density effects, and scenario results should therefore be interpreted in a relative rather than prescriptive sense.

We acknowledge that the calibration of EcoPlot-iso is subject to parameter equifinality, whereby multiple parameter combinations can reproduce the observed soil moisture and isotope dynamics with similarly good performance. Rather than seeking a single optimal parameter set, our calibration strategy explicitly accounts for this equifinality by propagating uncertainty from the 100 best-performing simulations into all key results. Uncertainty envelopes (5th–95th percentiles) shown in Figures 4, 6, and 8 illustrate the range of annual and seasonal flux responses, enabling the magnitude of parametric uncertainty to be evaluated relative to differences among forest types and management scenarios. Although parametric uncertainty is non-negligible and in some cases comparable to different forest management scenarios, the main findings are supported by consistent ensemble-mean responses and clear directional differences in water partitioning across scenarios. Accordingly,

results are interpreted in a relative and comparative sense, emphasizing management-relevant trade-offs rather than absolute flux predictions.

In the baseline simulations for ~~mature~~ broadleafved forest, conifer forest and agroforestry at the DMC site, the estimated mean annual evapotranspiration (ET) over ~~for or~~ 2000–2024 was 3960 ~~mm/year~~, 434, and 376 mm yr^{-1}, respectively, accounting for approximately 7223%, 80%, and 69% of annual precipitation. ~~This~~ These values ~~is~~ are consistent with ~~ET estimates reported in~~ previous modelling studies at the DMC ~~in 2021~~, which reported ET fractions ranging from 68% to over 80% of annual precipitation (Smith et al., 2021; Landgraf et al., 2023). ~~, 2018–2020 . The~~Difference among studies ~~discrepancy~~ may reflect interannual climate variability and the influence of particularly dry or wet years that ~~cannot~~ arebe not captured by short-term assessments. Differences ~~Differences~~ in model structure, parameterization, and input data may also contribute to the spread in reported ET values. In addition, to further assess model performance using an independent data source, simulated ET was evaluated against MODIS-derived ET for all land use sites in the DMC, including broadleaf forest, conifer forest, agroforestry, cropland, and grassland (Fig. S8 and Table S4). Model performance was quantified using KGE metrics calculated from daily ET, providing an external validation independent of the calibration data. While EcoPlot-iso tends to slightly underestimate ET relative to MODIS observations, KGE values indicate good agreement in temporal dynamics across land-use types, supporting the model's ability to reproduce key ET variability. ~~Nonetheless~~Overall, this evaluation ~~comparison~~ underscores the importance of long-term simulations and independent data-based validation for capturing representative ecohydrological ~~hydrological~~ behavior and for assessing ~~evaluating~~ the impacts of forest management strategies under variable climatic conditions.

In catchments like DMC, where evapotranspiration (ET) is high, atmospheric demand is the primary driver of root water uptake, though vegetation plays a key role in regulating its impact on water availability. In Brandenburg, coniferous forests have traditionally been favored on sandy soils, but modelling indicates high water use due to interception losses and year-round transpiration potential (Fig. S9c). Consequently, the implications for both reduced groundwater recharge and reduced forest productivity has encouraged landowners to explore alternative land use, such as broadleaves forests and agroforestry. These options have the potential for optimizing biomass productivity and land use resilience with increased landscape water retention and increased groundwater recharge.

These results (e.g., Figs. ~~7~~8 and S10~~8~~) have practical applications, such as estimating the direction and magnitude of the changes in evapotranspiration and water yield as a function of forest management practices, driven by alterations in canopy structure and rooting depth. The modelling approach thus provides useful insights into the hydrological implications of alternative canopy structures and rooting patterns for water use. Figure 12 compares the mean annual partitioning of water fluxes and soil moisture across broadleaf, coniferous, and agroforest types under dry and wet year conditions. It highlights how different vegetation strategies influence hydrological resilience, with substantial differences in water partitioning observed between dry and wet years across contrasting forest management scenarios. By simulating long-term water availability across periods of alternating wet and dry conditions, EcoPlot-iso simulations suggest that mixed forests and agroforestry can enhance water supply resilience in drought-sensitive catchments by sustaining both water yield and groundwater recharge.

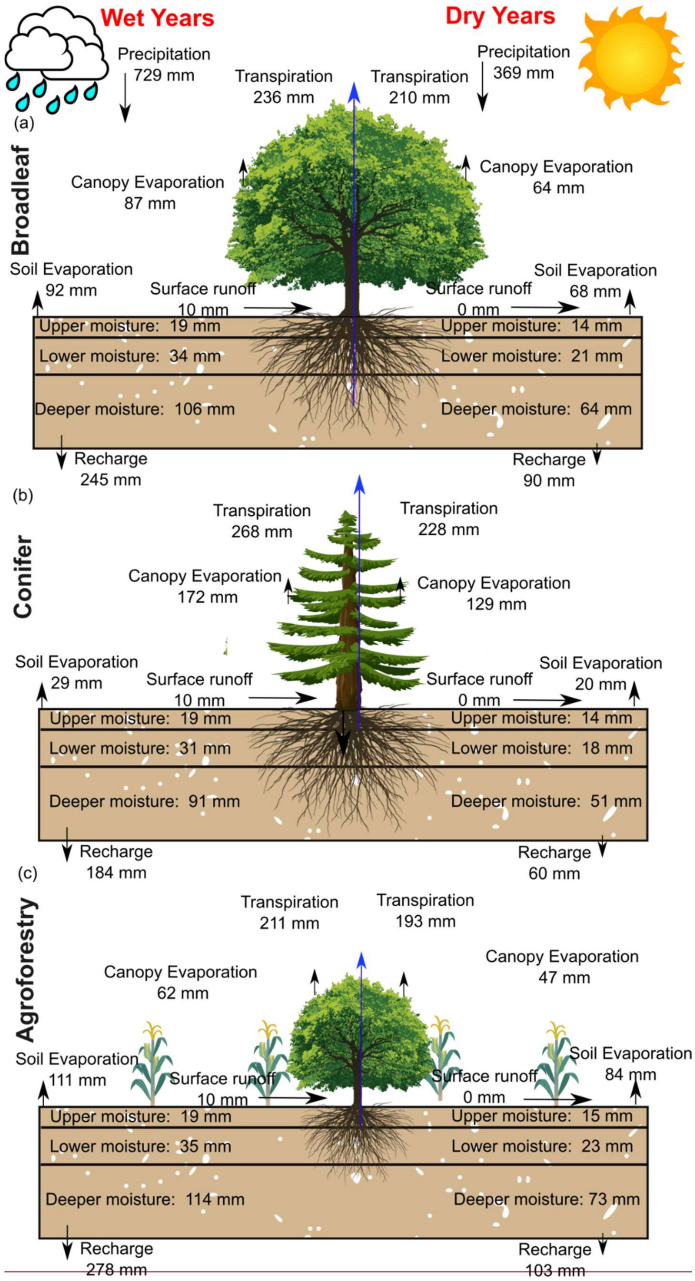
Wet Years
Dry Years
Precipitation
729 mm
Precipitation
369 mm
(a)
Broadleaf
Transpiration
236 mm
Transpiration
210 mm
Canopy Evaporation
87 mm
Canopy Evaporation
64 mm
Soil Evaporation
92 mm
Surface runoff
10 mm
Surface runoff
0 mm
Soil Evaporation
68 mm
Upper moisture: 19 mm
Upper moisture: 14 mm
Lower moisture: 34 mm
Lower moisture: 21 mm
Deeper moisture: 106 mm
Deeper moisture: 64 mm
Recharge
245 mm
Recharge
90 mm
(b)
Conifer
Transpiration
268 mm
Transpiration
228 mm
Canopy Evaporation
172 mm
Canopy Evaporation
129 mm
Soil Evaporation
29 mm
Surface runoff
10 mm
Surface runoff
0 mm
Soil Evaporation
20 mm
Upper moisture: 19 mm
Upper moisture: 14 mm
Lower moisture: 31 mm
Lower moisture: 18 mm
Deeper moisture: 91 mm
Deeper moisture: 51 mm
Recharge
184 mm
Recharge
60 mm
(c)
Agroforestry
Transpiration
211 mm
Transpiration
193 mm
Canopy Evaporation
62 mm
Canopy Evaporation
47 mm
Soil Evaporation
111 mm
Surface runoff
10 mm
Surface runoff
0 mm
Soil Evaporation
84 mm
Upper moisture: 19 mm
Upper moisture: 15 mm
Lower moisture: 35 mm
Lower moisture: 23 mm
Deeper moisture: 114 mm
Deeper moisture: 73 mm
Recharge
278 mm
Recharge
103 mm

827

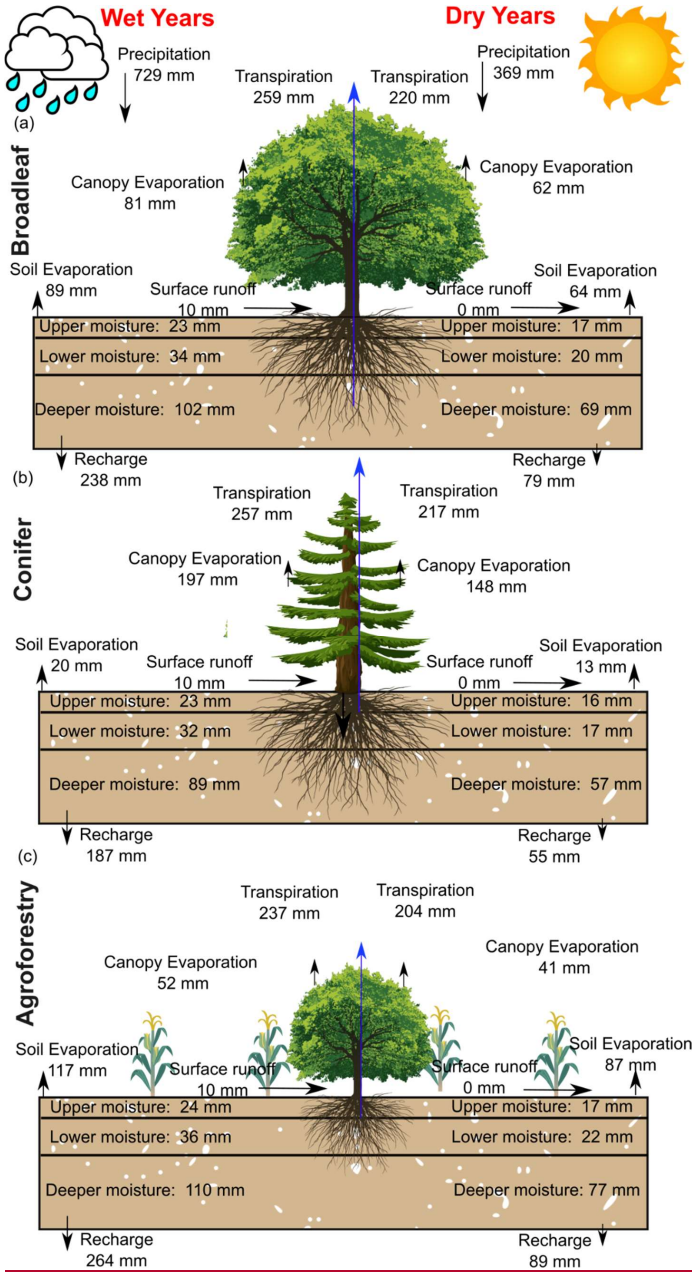

Figure 122. Comparison of mean annual water fluxes and soil moisture in the upper, lower, and deeper layers for Broadleaf (a), Coniferous (b), and Agroforest (c) forests under dry (2006, 2018, 2022) and wet (2002, 2007, 2010, 2023) year conditions.

5.2 ~~Soil~~ Soil Moisture Dynamics and Root Water Uptake Processes across Forest Management Scenarios ~~Moisture Anomalies and Their Implications for Resilience~~

At most of the monitoring plots in the DMC, groundwater is typically more than 3 meters below the ground surface (Ying et al., 2025). Therefore, except in older forest plots with deeply rooting trees, vegetation relies on soil moisture for root water uptake. Even for mature trees, there is evidence that most root water uptake occurs in the near-surface soil horizons, as demonstrated by ~~(~~Birkel et al.~~,~~ (2025), 20 km from the DMC. A global synthesis by ~~(~~Evaristo & McDonnell~~,~~ (2017) further supports this, indicating that ~77% of plant water uptake comes from shallow sources, with deeper groundwater use primarily in more arid regions. While hydraulic redistribution may provide deeper access for some species (Emerman & Dawson, 1996), rooting strategies are complex and highly species-specific (Demir et al., 2024). In this context, our results highlight the intermediate soil layer (10–30 cm) as the most reactive and significant for sustaining transpiration, with anomaly magnitudes nearly twice those of both the shallow (0–10 cm) and deeper (30–60 cm) layers across all forest types.

In addition, seasonal comparisons revealed that summer soil moisture anomalies were more negative than those in spring for all forest types (Fig.~~ure~~ S12~~5~~). This is likely linked to higher temperatures and evapotranspiration during summer, which intensify water stress and drive seasonal variation in soil moisture availability. Forest density and rooting characteristics substantially influenced the relative magnitude of soil moisture anomalies (Figs.~~ure~~ S6~~1~~3 and S7~~1~~4, respectively). Denser forests exhibited stronger negative anomalies during dry periods and enhanced positive anomalies in wet periods, amplifying seasonal fluctuations. For example, high-density (LAI scaling factor 1.6) conifer stands showed relative anomalies up to 25% greater than their low-density counterparts (Fig.~~ure~~ S14~~7~~). In contrast, shallow-rooted systems moderated this response, leading to more stable soil moisture dynamics. Among the management scenarios, agroforestry consistently exhibited the smallest anomalies, reflecting greater buffering capacity and higher ecohydrological resilience.

The improved rooting scheme in EcoPlot-iso represents depth-dependent transpiration by dynamically linking root water uptake efficiency to soil moisture availability across three soil compartments (see Section 3.2). Unlike models such as RHESSys and EcH2O, which partition a prescribed total transpiration—typically derived from the energy balance—across layers based on static root distributions, our approach allows transpiration to emerge from potential evapotranspiration, root-zone constraints, and soil moisture availability. The aim was not to optimize species-specific root dynamics, but to represent the relative influence of rooting depth on water uptake and partitioning, particularly in shallow-rooted or structurally diverse systems such as young forests. While the new implementation improves the process representation of root–soil interactions, it did not result in a substantial improvement in simulated soil moisture. For shallow vegetation types such as grasslands and croplands, model performance—measured using the mKGE was similar with and without the new transpiration function (results not shown). Moreover, direct validation of the root uptake scheme remains challenging due to the lack of supporting observations, such as root distribution data, xylem water isotopes, or sap flux measurements. Addressing this issue is a clear priority for future research.

These findings highlight how structurally diverse systems, such as agroforests, enhance the buffering capacity of ecosystems by improving groundwater recharge and reducing the amplitude of soil moisture fluctuations, thereby supporting greater resilience during dry periods (Tetzlaff et al., 2024). Together, these insights underscore the importance of rooting depth, forest structure, and seasonal climate variability in shaping soil moisture patterns

and regulating vegetation resilience. Accounting for these factors is essential for informing adaptive forest management in drought-prone catchments like the DMC.

5.3 Advancing Tracer-Aided Ecohydrological ~~Modeling~~Modelling: Challenges and Future Outlook

This study demonstrates that tracer-aided ecohydrological models, such as the isotope-aided EcoPlot-iso, can be used to effectively quantify the impact of forest management scenarios on water partitioning and ecohydrological resilience. By distinguishing between evaporation, transpiration, and subsurface water movements using stable isotopes (Soulsby et al., 2015), the model captures key hydrological responses—including evapotranspiration (ET), groundwater recharge, and soil moisture dynamics—under varying management strategies. These insights support evidence-based decision-making in drought-sensitive landscapes.

Despite these advances, several challenges remain. Conducted in a 66 km² mid-sized basin, this study did not include land use change induced atmospheric feedbacks—such as changes in albedo, radiative balance, or rainfall patterns—which are less critical at this scale but become important in larger-scale modeling (Ellison et al., 2012; Filoso et al., 2017). Moreover, this study applied a multi-objective calibration approach, combined with Monte Carlo sampling, that equally weighted isotopic and soil moisture data. However, further investigation is needed in how these observational constraints are balanced and interpreted. Recent advances—such as the DREAM(LoAX) framework (Wu et al., 2025)—demonstrate how simultaneous calibration and diagnostic analysis under the equifinality thesis can improve parameter identifiability, model robustness, and process understanding in tracer-aided ecohydrological models.

While this study used ~~relies on~~ δ^2H to constrain evaporative fractionation given~~-~~, the combined use of $\delta^{18}O$ and δ^2H (or d-excess) may help~~could further~~ improve the separation of evaporation effects and mixing processes (e.g. Penna et al., 2018) though this was beyond the scope of this paper~~and represents an important direction for future tracer-aided model development within EcoPlot-iso.~~ Many recent studies have used isotopic data to investigate root water uptake patterns, revealing how tree species, soil properties, and spatial water availability shape plant water use strategies (Demir et al., 2024; Rothfuss & Javaux, 2017). Integrating tracer-aided models with soil and xylem water isotope data offers a promising path to improving the representation of root water uptake, which is often simplified in current modelling approaches (Birkel et al., 2025). Improving root uptake representation requires consideration of species-specific traits and local soil-water conditions. However, the practical application of such improvements is limited by the scarcity of soil and xylem water isotope data, which are essential for constraining root water uptake dynamics but remain rare due to the labor-intensive and technically demanding nature of field sampling and laboratory analysis (Landgraf et al., 2022; Sprenger et al., 2017). This scarcity hinders the spatial and temporal resolution of observational data, limiting our ability to refine root water uptake processes in tracer-aided models.

Upscaling from plot to landscape level remains complex due to spatial heterogeneity in vegetation, soils, and topography. Addressing this requires spatially distributed modeling frameworks that can explicitly capture heterogeneity in ecohydrological processes across different landscape units (Kuppel et al., 2018; van Huijgevoort et al., 2016). Enhanced integration with remote sensing techniques can also help address these scaling limitations by providing spatially continuous data on vegetation dynamics, soil moisture, and ET (Yang et al., 2023). Incorporating ET observations, for instance, could strengthen model interpretation of flux dynamics. Currently,

key processes such as lateral subsurface flows and upward capillary fluxes are not explicitly represented in the EcoPlot-iso model. Including these components, along with improved representation of groundwater-surface water interactions, could improve simulations of water connectivity and storage resilience.

It is important to note that the scenario framework presented here is intentionally exploratory and management-oriented, rather than species-specific. While EcoPlot-iso captures key controls on water partitioning through canopy structure, soil moisture dynamics, and tracer-based separation of fluxes, additional physiological traits—such as stomatal regulation, vapor pressure deficit (VPD) sensitivity, and species-specific drought stress strategies—are not explicitly represented. These processes are known to influence transpiration dynamics and vegetation responses to drought, and their inclusion represents an important direction for future model development. Accordingly, the results of this study are interpreted in a relative sense, emphasizing comparative responses and management-relevant trade-offs rather than absolute or species-level predictions.

~~Future development should emphasize the coupling of tracer-based approaches with high-resolution hydrological modeling, remote sensing data, isotope data, and empirical field studies. Such interdisciplinary integration is essential for improving the scalability and applicability of tracer-aided ecohydrological models, especially for informing sustainable forest and water management under uncertain hydroclimatic futures.~~

6 Conclusion and Outlook

The tracer~~isotope~~-aided ecohydrological model EcoPlot-iso ~~modelling framework~~ was applied to quantify ~~the~~ how ~~impacts~~ alternative~~of different~~ forest management ~~strategies~~ scenarios influence ~~on~~ long-term water partitioning and ecohydrological resilience in the drought-sensitive Demnitzer Millcreek catchment (DMC), ~~in~~ northeastern Germany. ~~The model was first set up and evaluated under a b~~Baseline simulations for the period 2000–2024 were established at three forest sites (broadleaf forest, conifer forest, and agroforestry) and successfully reproduced observed soil moisture and soil water isotope (δ^2H) dynamics through a multi-criteria calibration approach~~t a broadleaf reference site, successfully reproducing observed soil moisture and soil water isotope dynamics using a multi-objective calibration approach~~. A key development in this study was the integration of a depth-dependent root water uptake function, which enable the representation of transpiration across soil layers associated with contrasting rooting distributions and stand ages.~~A novel depth-dependent root water uptake function was integrated, and a suite of s~~ Building on these baseline simulations, a generic scenario framework was applied to systematically assess the effects of forest type, forest density, and rooting characteristics on evapotranspiration, groundwater recharge, and soil moisture dynamics under contrasting dry and wet climatic conditions.~~cenario simulations varying in forest type, canopy density, and rooting depth was conducted to assess changes in evapotranspiration, groundwater recharge, and soil moisture anomalies under both dry and wet climatic conditions.~~

The results revealed clear trade-offs between evapotranspiration (ET) and groundwater recharge across different ~~, depending on~~ forest management ~~strategies~~scenarios. On average, ~~Coniferou~~conifers forests ~~intensified drought impacts~~exhibited higher ET, ~~with~~ approximately 78–11~~13~~% ~~higher ET compared to~~greater than broadleaf forest and agroforestry ~~systems, and significantly~~, accompanied by reduced groundwater recharge, particularly during low-flow ~~dry~~ periods. In contrast, agroforestry ~~systems effectively~~ buffered drought stress, ~~and~~ maintain~~ed~~ing lower soil moisture variability, ~~which~~ and enhanced ~~simultaneously lowering ET and enhancing~~ groundwater

recharge ~~by about 13%~~. ~~Further analysis highlighted contrasting ecosystem responses: c~~Conifers showed the strongest soil moisture anomalies, indicating greater drought sensitivity, while agroforests exhibited the most stable soil water storage. The intermediate soil layer (10–30 cm) was identified as the most responsive zone, consistently exhibiting the largest anomalies due to its role as the dominant root water uptake region supporting transpiration.

Beyond advancing process understanding, this study provided a practical and transferable framework ~~tools~~ for land management. By incorporating key controls such as canopy properties and root distribution, EcoPlot-iso facilitates an accessible means of assessing long-term land management impacts on landscape ecohydrology. The visualization and decision-support framework developed here offers a transparent, scenario-based platform for evaluating forest management strategies in climate-sensitive regions. These tools are well-suited for informing resilient land use planning under increasing climate variability.

Looking ahead, future research could usefully aim to incorporate additional isotopic tracers—such as deeper soil water (> 1 m), groundwater, and xylem water isotopes—to further constrain root water uptake functions and capture their variability across species and hydroclimatic conditions. The integration of high-resolution remote sensing data—particularly LiDAR for detailed characterization of forest structure—will enhance model parameterization and improve the spatial representation of heterogeneity in canopy height, leaf area distribution, and forest density. Advancing the EcoPlot-iso framework to incorporate lateral subsurface flows, groundwater dynamics, and coupled land–atmosphere feedbacks will support broader applications, including the assessment of large-scale land use change. Collectively, these developments will enhance model robustness and enable more informed, resilient land and water management strategies under a warming climate.

Code and data availability

The data and code that support the findings of this study are available from the corresponding author upon reasonable request.

Author contribution

CJ contributed to the methodology, software development, formal analysis, investigation, visualization, and writing of the original draft. DT contributed to conceptualization, investigation, data curation, validation, resources, project administration, and funding acquisition. SW contributed to methodology, investigation and data curation. CB contributed to software, methodology, and resources. HL contributed to investigation, visualization and validation. CS contributed to conceptualization, methodology, validation, investigation. All authors contributed to writing – review and editing.

Competing interests

The authors declare that they have no conflict of interest.

Acknowledgements

Tetzlaff's contributions were partly funded through the WETSCAPES2.0 project (DFG TRR410/1 2025). Tetzlaff also received funding from the "Wasserressourcenpreis 2024" awarded by the Rüdiger Kurt Bode-Foundation. Contributions from Soulsby were supported by Leibnitz Association Germany in the project Wetland Restoration in Peatlands. Laudon was funded by KAW 2018.0259 and 2023.0245, and Soulsby was also funded as an International KSLA Guest Professor at SLU by the Wallenberg Foundation (WP2023-0001). Birkel would like to thank the IGB for generously supporting him with a senior fellowship and the UCR for a sabbatical license. We extend our appreciation to Benedikt Boesel and the team from the Finck Foundation (www.finck-stiftung.org) for their collaborative support and for granting access to study sites. The authors are very grateful for the constructive comments provided by the Editor, Prof. Dr. Anke Hildebrandt, and two anonymous reviewers.

Reference

Ault, T. R. (2020). On the essentials of drought in a changing climate. In *Science* (Vol. 368, Number 6488). https://doi.org/10.1126/science.aaz5492

Birkel, C., Arciniega-Esparza, S., Maneta, M. P., Boll, J., Stevenson, J. L., Benegas-Negri, L., Tetzlaff, D., & Soulsby, C. (2024). Importance of measured transpiration fluxes for modelled ecohydrological partitioning in a tropical agroforestry system. *Agricultural and Forest Meteorology*, *346*. https://doi.org/10.1016/j.agrformet.2023.109870

Birkel, C., Tetzlaff, D., Ring, A. M., & Soulsby, C. (2025). Does high resolution in situ xylem and atmospheric vapor isotope data help improve modeled estimates of ecohydrological partitioning? *Agricultural and Forest Meteorology*, *365*. https://doi.org/10.1016/j.agrformet.2025.110467

Bonan, G. B. (2008). Forests and climate change: Forcings, feedbacks, and the climate benefits of forests. In *Science* (Vol. 320, Number 5882). https://doi.org/10.1126/science.1155121

Bosch, J. M., & Hewlett, J. D. (1982). A REVIEW OF CATCHMENT EXPERIMENTS TO DETERMINE THE EFFECT OF VEGETATION CHANGES ON WATER YIELD AND EVAPOTRANSPIRATION. In *Journal of Hydrology* (Vol. 55).

Brauman, K. A., Freyberg, D. L., & Daily, G. C. (2010). Forest structure influences on rainfall partitioning and cloud interception: A comparison of native forest sites in Kona, Hawai'i. *Agricultural and Forest Meteorology*, *150*(2). https://doi.org/10.1016/j.agrformet.2009.11.011

Brown, A. E., Western, A. W., McMahon, T. A., & Zhang, L. (2013). Impact of forest cover changes on annual streamflow and flow duration curves. *Journal of Hydrology*, *483*. https://doi.org/10.1016/j.jhydrol.2012.12.031

Brown, A. E., Zhang, L., McMahon, T. A., Western, A. W., & Vertessy, R. A. (2005). A review of paired catchment studies for determining changes in water yield resulting from alterations in vegetation. *Journal of Hydrology*, *310*(1–4), 28–61. https://doi.org/10.1016/j.jhydrol.2004.12.010

Calder, I. R. (1998). Water use by forests, limits and controls. *Tree Physiology*, *18*(8–9). https://doi.org/10.1093/treephys/18.8-9.625

Demir, G., Guswa, A. J., Filipzik, J., Metzger, J. C., Römermann, C., & Hildebrandt, A. (2024). Root water uptake patterns are controlled by tree species interactions and soil water variability. *Hydrology and Earth System Sciences*, *28*(6), 1441–1461. https://doi.org/10.5194/hess-28-1441-2024

Douinot, A., Tetzlaff, D., Maneta, M., Kuppel, S., Schulte-Bisping, H., & Soulsby, C. (2019). Ecohydrological modelling with EcH2O-iso to quantify forest and grassland effects on water partitioning and flux ages. *Hydrological Processes*, *33*(16), 2174–2191. https://doi.org/10.1002/hyp.13480

Dubbert, M., Couvreur, V., Kübert, A., & Werner, C. (2023). Plant water uptake modelling: added value of cross-disciplinary approaches. In *Plant Biology* (Vol. 25, Number 1). https://doi.org/10.1111/plb.13478

Ellison, D., Futter, M. N., & Bishop, K. (2012). On the forest cover-water yield debate: From demand- to supply-side thinking. In *Global Change Biology* (Vol. 18, Number 3). https://doi.org/10.1111/j.1365-2486.2011.02589.x

Emerman, S. H., & Dawson, T. E. (1996). Hydraulic lift and its influence on the water content of the rhizosphere: An example from sugar maple, Acer saccharum. *Oecologia*, *108*(2). https://doi.org/10.1007/BF00334651

Estrela, T., & Vargas, E. (2012). Drought Management Plans in the European Union. The Case of Spain. In *Water Resources Management* (Vol. 26, Number 6). https://doi.org/10.1007/s11269-011-9971-2

Evaristo, J., & McDonnell, J. J. (2017). Prevalence and magnitude of groundwater use by vegetation: A global stable isotope meta-analysis. *Scientific Reports*, *7*. https://doi.org/10.1038/srep44110

Falkenmark, M., & Rockström, J. (2006). The New Blue and Green Water Paradigm: Breaking New Ground for Water Resources Planning and Management. *Journal of Water Resources Planning and Management*, *132*(3). https://doi.org/10.1061/(asce)0733-9496(2006)132:3(129)

Fatichi, S., Ivanov, V. Y., & Caporali, E. (2012). A mechanistic ecohydrological model to investigate complex interactions in cold and warm water-controlled environments: 1. Theoretical framework and plot-scale analysis. *Journal of Advances in Modeling Earth Systems*, *4*(5). https://doi.org/10.1029/2011MS000086

Filoso, S., Bezerra, M. O., Weiss, K. C. B., & Palmer, M. A. (2017). Impacts of forest restoration on water yield: A systematic review. In *PLoS ONE* (Vol. 12, Number 8). https://doi.org/10.1371/journal.pone.0183210

Gelbrecht, J., Driescher, E., Lademann, H., Schönfelder, J., & Exner, H.-J. (1996). Diffuse nutrient impact on surface water bodies and its abatement by restoration measures in a small catchment area in North-East Germany. *Water Science and Technology*, *33*(4–5). https://doi.org/10.2166/wst.1996.0501

Gelbrecht, J., Lengsfeld, H., Pöthig, R., & Opitz, D. (2005). Temporal and spatial variation of phosphorus input, retention and loss in a small catchment of NE Germany. *Journal of Hydrology*, *304*(1–4), 151–165. https://doi.org/10.1016/j.jhydrol.2004.07.028

Geris, J., Tetzlaff, D., Mcdonnell, J., & Soulsby, C. (2015). The relative role of soil type and tree cover on water storage and transmission in northern headwater catchments. *Hydrological Processes*, *29*(7). https://doi.org/10.1002/hyp.10289

Guswa, A. J., Tetzlaff, D., Selker, J. S., Carlyle-Moses, D. E., Boyer, E. W., Bruen, M., Cayuela, C., Creed, I. F., van de Giesen, N., Grasso, D., Hannah, D. M., Hudson, J. E., Hudson, S. A., Iida, S., Jackson, R. B., Katul, G. G., Kumagai, T., Llorens, P., Lopes Ribeiro, F., … Levia, D. F. (2020). Advancing ecohydrology in the 21st century: A convergence of opportunities. In *Ecohydrology* (Vol. 13, Number 4). John Wiley and Sons Ltd. https://doi.org/10.1002/eco.2208

Hersbach, H., Bell, B., Berrisford, P., Hirahara, S., Horányi, A., Muñoz-Sabater, J., Nicolas, J., Peubey, C., Radu, R., Schepers, D., Simmons, A., Soci, C., Abdalla, S., Abellan, X., Balsamo, G., Bechtold, P., Biavati, G., Bidlot, J., Bonavita, M., … Thépaut, J.-N. (2020). The ERA5 global reanalysis. *Quarterly Journal of the Royal Meteorological Society*, *146*(730), 1999–2049. https://doi.org/https://doi.org/10.1002/qj.3803

Hibbert, A. R. (1967). Forest Treatment Effects on Water Yield. *International Symposium For Hydrology*.

Huntington, T. G. (2006). Evidence for intensification of the global water cycle: Review and synthesis. *Journal of Hydrology*, *319*(1–4), 83–95. https://doi.org/10.1016/j.jhydrol.2005.07.003

Kleine, L., Tetzlaff, D., Smith, A., Dubbert, M., & Soulsby, C. (2021). Modelling ecohydrological feedbacks in forest and grassland plots under a prolonged drought anomaly in Central Europe 2018–2020. *Hydrological Processes*, *35*(8). https://doi.org/10.1002/hyp.14325

Kling, H., Fuchs, M., & Paulin, M. (2012). Runoff conditions in the upper Danube basin under an ensemble of climate change scenarios. *Journal of Hydrology*, *424–425*. https://doi.org/10.1016/j.jhydrol.2012.01.011

Knighton, J., Kuppel, S., Smith, A., Soulsby, C., Sprenger, M., & Tetzlaff, D. (2020). Using isotopes to incorporate tree water storage and mixing dynamics into a distributed ecohydrologic modelling framework. *Ecohydrology*, *13*(3). https://doi.org/10.1002/eco.2201

Knighton, J., Sanchez-Martinez, P., & Anderegg, L. (2024). A global dataset of tree hydraulic and structural traits imputed from phylogenetic relationships. *Scientific Data* , *11*(1). https://doi.org/10.1038/s41597-024-04254-4

Kool, D., Agam, N., Lazarovitch, N., Heitman, J. L., Sauer, T. J., & Ben-Gal, A. (2014). A review of approaches for evapotranspiration partitioning. In *Agricultural and Forest Meteorology* (Vol. 184). https://doi.org/10.1016/j.agrformet.2013.09.003

Kumar, R., Shankar, V., & Jat, M. K. (2015). Evaluation of root water uptake models - A review. In *ISH Journal of Hydraulic Engineering* (Vol. 21, Number 2). https://doi.org/10.1080/09715010.2014.981955

Kuppel, S., Tetzlaff, D., Maneta, M. P., & Soulsby, C. (2018). EcH2O-iso 1.0: Water isotopes and age tracking in a process-based, distributed ecohydrological model. *Geoscientific Model Development*, *11*(7), 3045–3069. https://doi.org/10.5194/gmd-11-3045-2018

Landgraf, J., Tetzlaff, D., Birkel, C., Stevenson, J. L., & Soulsby, C. (2023). Assessing land use effects on ecohydrological partitioning in the critical zone through isotope-aided modelling. *Earth Surface Processes and Landforms*, *48*(15), 3199–3219. https://doi.org/10.1002/esp.5691

Landgraf, J., Tetzlaff, D., Wu, S., Freymüller, J., & Soulsby, C. (2022). Using stable water isotopes to understand ecohydrological partitioning under contrasting land uses in a drought-sensitive rural, lowland catchment. *Hydrological Processes*, *36*(12). https://doi.org/10.1002/hyp.14779

Luo, S., Tetzlaff, D., Smith, A., & Soulsby, C. (2024). Assessing impacts of alternative land use strategies on water partitioning, storage and ages in drought-sensitive lowland catchments using tracer-aided ecohydrological modelling. *Hydrological Processes*, *38*(4). https://doi.org/10.1002/hyp.15126

Mahmood, R., Pielke, R. A., Hubbard, K. G., Niyogi, D., Dirmeyer, P. A., Mcalpine, C., Carleton, A. M., Hale, R., Gameda, S., Beltrán-Przekurat, A., Baker, B., Mcnider, R., Legates, D. R., Shepherd, M., Du, J., Blanken, P. D., Frauenfeld, O. W., Nair, U. S., & Fall, S. (2014). Land cover changes and their biogeophysical effects on climate. *International Journal of Climatology*, *34*(4). https://doi.org/10.1002/joc.3736

McKay, M. D., Beckman, R. J., & Conover, W. J. (1979). Comparison of three methods for selecting values of input variables in the analysis of output from a computer code. *Technometrics*, *21*(2). https://doi.org/10.1080/00401706.1979.10489755

Neill, A. J., Birkel, C., Maneta, M. P., Tetzlaff, D., & Soulsby, C. (2021). Structural changes to forests during regeneration affect water flux partitioning, water ages and hydrological connectivity: Insights from tracer-aided ecohydrological modelling. *Hydrology and Earth System Sciences*, *25*(9), 4861–4886. https://doi.org/10.5194/hess-25-4861-2021

Orth, R., & Destouni, G. (2018). Drought reduces blue-water fluxes more strongly than green-water fluxes in Europe. *Nature Communications*, *9*(1). https://doi.org/10.1038/s41467-018-06013-7

Penna, D., Hopp, L., Scandellari, F., Allen, S. T., Benettin, P., Beyer, M., Geris, J., Klaus, J., Marshall, J. D., Schwendenmann, L., Volkmann, T. H. M., Von Freyberg, J., Amin, A., Ceperley, N., Engel, M., Frentress, J., Giambastiani, Y., McDonnell, J. J., Zuecco, G., … Kirchner, J. W. (2018). Ideas and perspectives: Tracing terrestrial ecosystem water fluxes using hydrogen and oxygen stable isotopes - Challenges and opportunities from an interdisciplinary perspective. *Biogeosciences*, *15*(21). https://doi.org/10.5194/bg-15-6399-2018

Pielke, R. A., Pitman, A., Niyogi, D., Mahmood, R., McAlpine, C., Hossain, F., Goldewijk, K. K., Nair, U., Betts, R., Fall, S., Reichstein, M., Kabat, P., & de Noblet, N. (2011). Land use/land cover changes and climate: Modeling analysis and observational evidence. In *Wiley Interdisciplinary Reviews: Climate Change* (Vol. 2, Number 6). https://doi.org/10.1002/wcc.144

Quandt, A., Neufeldt, H., & Gorman, K. (2023). Climate change adaptation through agroforestry: opportunities and gaps. In *Current Opinion in Environmental Sustainability* (Vol. 60). https://doi.org/10.1016/j.cosust.2022.101244

Ricci, G. F., De Girolamo, A. M., & Gentile, F. (2020). Modeling the Effect of Different Management Practices for Soil Erosion Control in a Mediterranean Watershed. *Lecture Notes in Civil Engineering*, *67*(June), 125–132. https://doi.org/10.1007/978-3-030-39299-4_14

Rothfuss, Y., & Javaux, M. (2017). Reviews and syntheses: Isotopic approaches to quantify root water uptake: A review and comparison of methods. *Biogeosciences*, *14*(8). https://doi.org/10.5194/bg-14-2199-2017

Shen, H., Tolson, B. A., & Mai, J. (2022). Time to Update the Split-Sample Approach in Hydrological Model Calibration. *Water Resources Research*, *58*(3). https://doi.org/10.1029/2021WR031523

Smith, A., Tetzlaff, D., Gelbrecht, J., Kleine, L., & Soulsby, C. (2020). Riparian wetland rehabilitation and beaver re-colonization impacts on hydrological processes and water quality in a lowland agricultural catchment. *Science of the Total Environment*, *699*. https://doi.org/10.1016/j.scitotenv.2019.134302

Smith, A., Tetzlaff, D., Kleine, L., Maneta, M., & Soulsby, C. (2021). Quantifying the effects of land use and model scale on water partitioning and water ages using tracer-aided ecohydrological models. *Hydrology and Earth System Sciences*, *25*(4), 2239–2259. https://doi.org/10.5194/hess-25-2239-2021

Soulsby, C., Birkel, C., Geris, J., Dick, J., Tunaley, C., & Tetzlaff, D. (2015). Stream water age distributions controlled by storage dynamics and nonlinear hydrologic connectivity: Modeling with high-resolution isotope data. *Water Resources Research*, *51*(9). https://doi.org/10.1002/2015WR017888

Sprenger, M., Tetzlaff, D., & Soulsby, C. (2017). Soil water stable isotopes reveal evaporation dynamics at the soil-plant-atmosphere interface of the critical zone. *Hydrology and Earth System Sciences*, *21*(7). https://doi.org/10.5194/hess-21-3839-2017

Sterling, S. M., Ducharne, A., & Polcher, J. (2013). The impact of global land-cover change on the terrestrial water cycle. *Nature Climate Change*, *3*(4). https://doi.org/10.1038/nclimate1690

Stevenson, J. L., Birkel, C., Comte, J. C., Tetzlaff, D., Marx, C., Neill, A., Maneta, M., Boll, J., & Soulsby, C. (2023). Quantifying heterogeneity in ecohydrological partitioning in urban green spaces through the integration of empirical and modelling approaches. *Environmental Monitoring and Assessment*, *195*(4). https://doi.org/10.1007/s10661-023-11055-6

Tague, C. L., & Band, L. E. (2004). RHESSys: Regional Hydro-Ecologic Simulation System—An Object-Oriented Approach to Spatially Distributed Modeling of Carbon, Water, and Nutrient Cycling. *Earth Interactions*, *8*(19). https://doi.org/10.1175/1087-3562(2004)8<1:rrhsso>2.0.co;2

Tetzlaff, D., Carey, S. K., McNamara, J. P., Laudon, H., & Soulsby, C. (2017). The essential value of long-term experimental data for hydrology and water management. In *Water Resources Research* (Vol. 53, Number 4, pp. 2598–2604). Blackwell Publishing Ltd. https://doi.org/10.1002/2017WR020838

Tetzlaff, D., Laudon, H., Luo, S., & Soulsby, C. (2024). Ecohydrological resilience and the landscape water storage continuum in droughts. *Nature Water*, *2*(10), 915–918. https://doi.org/10.1038/s44221-024-00300-y

te Wierik, S. A., Cammeraat, E. L. H., Gupta, J., & Artzy-Randrup, Y. A. (2021). Reviewing the Impact of Land Use and Land-Use Change on Moisture Recycling and Precipitation Patterns. In *Water Resources Research* (Vol. 57, Number 7). https://doi.org/10.1029/2020WR029234

Trenberth, K. E. (2011). Changes in precipitation with climate change. *Climate Research*, *47*(1–2), 123–138. https://doi.org/10.3354/cr00953

van Huijgevoort, M. H. J., Tetzlaff, D., Sutanudjaja, E. H., & Soulsby, C. (2016). Using high resolution tracer data to constrain water storage, flux and age estimates in a spatially distributed rainfall-runoff model. *Hydrological Processes*, *30*(25), 4761–4778. https://doi.org/10.1002/hyp.10902

Formatted: German (Germany)

Wang-Erlandsson, L., Van Der Ent, R. J., Gordon, L. J., & Savenije, H. H. G. (2014). Contrasting roles of interception and transpiration in the hydrological cycle - Part 1: Temporal characteristics over land. *Earth System Dynamics*, *5*(2). https://doi.org/10.5194/esd-5-441-2014

Wu, S., Tetzlaff, D., Beven, K., & Soulsby, C. (2025). DREAM(LoAX): Simultaneous Calibration and Diagnosis for Tracer-Aided Ecohydrological Models Under the Equifinality Thesis. *Water Resources Research*, *61*(3), e2024WR038779. https://doi.org/https://doi.org/10.1029/2024WR038779

Wu, S., Tetzlaff, D., Goldhammer, T., & Soulsby, C. (2021). Hydroclimatic variability and riparian wetland restoration control the hydrology and nutrient fluxes in a lowland agricultural catchment. *Journal of Hydrology*, *603*. https://doi.org/10.1016/j.jhydrol.2021.126904

Wu, S., Tetzlaff, D., Yang, X., Smith, A., & Soulsby, C. (2023). Integrating Tracers and Soft Data Into Multi-Criteria Calibration: Implications From Distributed Modeling in a Riparian Wetland. *Water Resources Research*, *59*(11). https://doi.org/10.1029/2023WR035509

Yang, X., Tetzlaff, D., Müller, C., Knöller, K., Borchardt, D., & Soulsby, C. (2023). Upscaling Tracer-Aided Ecohydrological Modeling to Larger Catchments: Implications for Process Representation and Heterogeneity in Landscape Organization. *Water Resources Research*, *59*(3). https://doi.org/10.1029/2022WR033033

Ying, Z., Tetzlaff, D., Comte, J.-C., Wu, S., & Soulsby, C. (2025). Storage Dynamics and Groundwater–Surface Water Interactions in a Drought Sensitive Lowland Catchment: Process-Based Modelling as a Learning Tool. *Hydrological Processes*, *39*(5), e70141. https://doi.org/https://doi.org/10.1002/hyp.70141

Yuan, X., Wang, Y., Ji, P., Wu, P., Sheffield, J., & Otkin, J. A. (2023). A global transition to flash droughts under climate change. *Science*, *380*(6641). https://doi.org/10.1126/science.abn6301

Zhang, L., Dawes, W. R., & Walker, G. R. (2001). Response of mean annual evapotranspiration to vegetation changes at catchment scale. *Water Resources Research*, *37*(3). https://doi.org/10.1029/2000WR900325

Page 6: [1] Formatted	**Cong Jiang**	**2/8/2026 8:27:00 PM**

English (United States)

Page 6: [2] Formatted	**Cong Jiang**	**2/8/2026 8:27:00 PM**

English (United States)

Page 6: [3] Formatted	**Cong Jiang**	**2/8/2026 8:27:00 PM**

English (United States)

Page 6: [4] Formatted	**Cong Jiang**	**2/8/2026 8:27:00 PM**

English (United States)

Page 6: [5] Formatted	**Cong Jiang**	**2/8/2026 8:27:00 PM**

English (United States)

Page 6: [6] Formatted	**Cong Jiang**	**2/8/2026 8:27:00 PM**

English (United States)

Page 6: [7] Formatted	**Cong Jiang**	**2/8/2026 8:27:00 PM**

English (United States)

Page 6: [8] Formatted	**Cong Jiang**	**2/8/2026 8:27:00 PM**

English (United States)

Page 6: [9] Formatted	**Cong Jiang**	**2/8/2026 8:27:00 PM**

English (United States)

Page 6: [10] Formatted	**Cong Jiang**	**2/8/2026 8:27:00 PM**

English (United States)

Page 6: [11] Formatted	**Cong Jiang**	**2/8/2026 8:27:00 PM**

English (United States)

Page 6: [12] Formatted	**Cong Jiang**	**2/8/2026 8:27:00 PM**

English (United States)

Page 6: [13] Formatted	**Cong Jiang**	**2/8/2026 8:27:00 PM**

English (United States)

Page 6: [14] Formatted	**Cong Jiang**	**2/8/2026 8:27:00 PM**

English (United States)

Page 6: [15] Formatted **Cong Jiang** **2/8/2026 8:27:00 PM**

English (United States)

Page 6: [16] Formatted **Cong Jiang** **2/8/2026 8:27:00 PM**

English (United States)

Page 6: [17] Formatted **Cong Jiang** **2/8/2026 8:27:00 PM**

English (United States)

Page 6: [18] Formatted **Cong Jiang** **2/8/2026 8:27:00 PM**

English (United States)

Page 6: [19] Formatted **Cong Jiang** **2/8/2026 8:27:00 PM**

English (United States)

Page 6: [20] Formatted **Cong Jiang** **2/8/2026 8:27:00 PM**

English (United States)

Page 6: [21] Formatted **Cong Jiang** **2/8/2026 8:27:00 PM**

English (United States)

Page 6: [22] Formatted **Cong Jiang** **2/8/2026 8:27:00 PM**

English (United States)

Page 6: [23] Formatted **Cong Jiang** **2/8/2026 8:27:00 PM**

English (United States)

Page 6: [24] Formatted **Cong Jiang** **2/8/2026 8:27:00 PM**

English (United States)

Page 6: [25] Formatted **Cong Jiang** **2/13/2026 2:16:00 PM**

Font: 10 pt, Bold, Font color: Auto

Page 6: [26] Formatted **Cong Jiang** **2/13/2026 2:16:00 PM**

Normal, Indent: Left: 0"

Page 6: [27] Formatted **Cong Jiang** **2/13/2026 2:16:00 PM**

Font: 10 pt, Font color: Auto

Page 6: [28] Formatted **Cong Jiang** **2/10/2026 4:23:00 AM**

Font color: Auto

Page 6: [29] Formatted Table **Cong Jiang** **2/8/2026 1:01:00 PM**

Formatted Table

Page 6: [30] Formatted **Cong Jiang** **2/10/2026 4:23:00 AM**

Font color: Auto

Page 6: [31] Formatted **Cong Jiang** **2/10/2026 4:23:00 AM**

Font color: Auto

Page 6: [32] Formatted **Cong Jiang** **2/10/2026 4:23:00 AM**

Font: (Default) Times New Roman, 10 pt, English (United States)

Page 6: [32] Formatted **Cong Jiang** **2/10/2026 4:23:00 AM**

Font: (Default) Times New Roman, 10 pt, English (United States)

Page 6: [33] Formatted **Cong Jiang** **2/10/2026 4:23:00 AM**

Font: (Default) Times New Roman, 10 pt, English (United States)

Page 6: [33] Formatted **Cong Jiang** **2/10/2026 4:23:00 AM**

Font: (Default) Times New Roman, 10 pt, English (United States)

Page 6: [34] Formatted **Cong Jiang** **2/10/2026 4:23:00 AM**

Font: (Default) Times New Roman, 10 pt, English (United States)

Page 6: [34] Formatted **Cong Jiang** **2/10/2026 4:23:00 AM**

Font: (Default) Times New Roman, 10 pt, English (United States)

Page 6: [35] Formatted **Cong Jiang** **2/10/2026 4:23:00 AM**

Font: (Default) Times New Roman, 10 pt, English (United States)

Page 6: [35] Formatted **Cong Jiang** **2/10/2026 4:23:00 AM**

Font: (Default) Times New Roman, 10 pt, English (United States)

Page 6: [36] Formatted **Cong Jiang** **2/10/2026 4:23:00 AM**

Font: (Default) Times New Roman, 10 pt, English (United States)

Page 6: [36] Formatted **Cong Jiang** **2/10/2026 4:23:00 AM**

Font: (Default) Times New Roman, 10 pt, English (United States)

Page 6: [37] Formatted **Cong Jiang** **2/10/2026 4:23:00 AM**

Font: (Default) Times New Roman, 10 pt, English (United States)

Page 6: [37] Formatted **Cong Jiang** **2/10/2026 4:23:00 AM**

Font: (Default) Times New Roman, 10 pt, English (United States)

Page 6: [38] Formatted **Cong Jiang** **2/10/2026 4:23:00 AM**

Font: (Default) Times New Roman, 10 pt, English (United States)

Page 6: [38] Formatted **Cong Jiang** **2/10/2026 4:23:00 AM**

Font: (Default) Times New Roman, 10 pt, English (United States)

Page 6: [39] Formatted **Cong Jiang** **2/10/2026 4:23:00 AM**

Font: (Default) Times New Roman, 10 pt, English (United States)

Page 6: [39] Formatted **Cong Jiang** **2/10/2026 4:23:00 AM**

Font: (Default) Times New Roman, 10 pt, English (United States)

Page 6: [40] Formatted **Cong Jiang** **2/10/2026 4:23:00 AM**

Font: (Default) Times New Roman, 10 pt, English (United States)

Page 6: [40] Formatted **Cong Jiang** **2/10/2026 4:23:00 AM**

Font: (Default) Times New Roman, 10 pt, English (United States)

Page 6: [41] Formatted **Cong Jiang** **2/10/2026 4:23:00 AM**

Font: (Default) Times New Roman, 10 pt, English (United States)

Page 6: [41] Formatted **Cong Jiang** **2/10/2026 4:23:00 AM**

Font: (Default) Times New Roman, 10 pt, English (United States)

Page 6: [42] Formatted **Cong Jiang** **2/10/2026 4:23:00 AM**

Font: (Default) Times New Roman, 10 pt, English (United States)

Page 6: [42] Formatted **Cong Jiang** **2/10/2026 4:23:00 AM**

Font: (Default) Times New Roman, 10 pt, English (United States)

Page 6: [43] Formatted **Cong Jiang** **2/10/2026 4:23:00 AM**

Font: (Default) Times New Roman, 10 pt, English (United States)

Page 6: [43] Formatted **Cong Jiang** **2/10/2026 4:23:00 AM**

Font: (Default) Times New Roman, 10 pt, English (United States)

Page 6: [44] Formatted **Cong Jiang** **2/10/2026 4:23:00 AM**

Font color: Auto

Page 6: [45] Formatted Table **Cong Jiang** **2/8/2026 3:38:00 PM**

Formatted Table

Page 6: [46] Formatted **Cong Jiang** **2/10/2026 4:23:00 AM**

Font color: Auto

Page 6: [47] Formatted **Cong Jiang** **2/10/2026 4:23:00 AM**

Font color: Auto

Page 6: [48] Formatted **Cong Jiang** **2/10/2026 4:23:00 AM**

Font: (Default) Times New Roman, 10 pt, English (United States)

Page 6: [48] Formatted **Cong Jiang** **2/10/2026 4:23:00 AM**

Font: (Default) Times New Roman, 10 pt, English (United States)

Page 6: [49] Formatted **Cong Jiang** **2/10/2026 4:23:00 AM**

Font: (Default) Times New Roman, 10 pt, English (United States)

Page 6: [49] Formatted **Cong Jiang** **2/10/2026 4:23:00 AM**

Font: (Default) Times New Roman, 10 pt, English (United States)

Page 6: [50] Formatted **Cong Jiang** **2/10/2026 4:23:00 AM**

Font: (Default) Times New Roman, 10 pt, English (United States)

Page 6: [50] Formatted **Cong Jiang** **2/10/2026 4:23:00 AM**

Font: (Default) Times New Roman, 10 pt, English (United States)

Page 6: [51] Formatted **Cong Jiang** **2/10/2026 4:23:00 AM**

Font: (Default) Times New Roman, 10 pt, English (United States)

Page 6: [51] Formatted **Cong Jiang** **2/10/2026 4:23:00 AM**

Font: (Default) Times New Roman, 10 pt, English (United States)

Page 6: [52] Formatted **Cong Jiang** **2/10/2026 4:23:00 AM**

Font: (Default) Times New Roman, 10 pt, English (United States)

Page 6: [52] Formatted **Cong Jiang** **2/10/2026 4:23:00 AM**

Font: (Default) Times New Roman, 10 pt, English (United States)

Page 6: [53] Formatted **Cong Jiang** **2/10/2026 4:23:00 AM**

Font: (Default) Times New Roman, 10 pt, English (United States)

Page 6: [53] Formatted **Cong Jiang** **2/10/2026 4:23:00 AM**

Font: (Default) Times New Roman, 10 pt, English (United States)

Page 6: [54] Formatted **Cong Jiang** **2/10/2026 4:23:00 AM**

Font: (Default) Times New Roman, 10 pt, English (United States)

Page 6: [54] Formatted **Cong Jiang** **2/10/2026 4:23:00 AM**

Font: (Default) Times New Roman, 10 pt, English (United States)

Page 6: [55] Formatted **Cong Jiang** **2/10/2026 4:23:00 AM**

Font: (Default) Times New Roman, 10 pt, English (United States)

Page 6: [55] Formatted **Cong Jiang** **2/10/2026 4:23:00 AM**

Font: (Default) Times New Roman, 10 pt, English (United States)

Page 6: [56] Formatted **Cong Jiang** **2/10/2026 4:23:00 AM**

Font: (Default) Times New Roman, 10 pt, English (United States)

Page 6: [56] Formatted **Cong Jiang** **2/10/2026 4:23:00 AM**

Font: (Default) Times New Roman, 10 pt, English (United States)

Page 6: [57] Formatted **Cong Jiang** **2/10/2026 4:23:00 AM**

Font: (Default) Times New Roman, 10 pt, English (United States)

Page 6: [57] Formatted **Cong Jiang** **2/10/2026 4:23:00 AM**

Font: (Default) Times New Roman, 10 pt, English (United States)

Page 6: [58] Formatted **Cong Jiang** **2/10/2026 4:23:00 AM**

Font: (Default) Times New Roman, 10 pt, English (United States)

Page 6: [58] Formatted **Cong Jiang** **2/10/2026 4:23:00 AM**

Font: (Default) Times New Roman, 10 pt, English (United States)

Page 6: [59] Formatted **Cong Jiang** **2/10/2026 4:23:00 AM**

Font: (Default) Times New Roman, 10 pt, English (United States)

Page 6: [59] Formatted **Cong Jiang** **2/10/2026 4:23:00 AM**

Font: (Default) Times New Roman, 10 pt, English (United States)

Page 6: [60] Formatted **Cong Jiang** **2/10/2026 4:23:00 AM**

Font color: Auto

Page 6: [61] Formatted **Cong Jiang** **2/10/2026 4:23:00 AM**

Font color: Auto

Page 6: [61] Formatted **Cong Jiang** **2/10/2026 4:23:00 AM**

Font color: Auto

Page 6: [62] Formatted **Cong Jiang** **2/10/2026 4:23:00 AM**

Font: (Default) Times New Roman, 10 pt, English (United States)

Page 6: [62] Formatted **Cong Jiang** **2/10/2026 4:23:00 AM**

Font: (Default) Times New Roman, 10 pt, English (United States)

Page 6: [63] Formatted **Cong Jiang** **2/10/2026 4:23:00 AM**

Font: (Default) Times New Roman, 10 pt, English (United States)

Page 6: [63] Formatted **Cong Jiang** **2/10/2026 4:23:00 AM**

Font: (Default) Times New Roman, 10 pt, English (United States)

Page 6: [64] Formatted **Cong Jiang** **2/10/2026 4:23:00 AM**

Font: (Default) Times New Roman, 10 pt, English (United States)

Page 6: [64] Formatted **Cong Jiang** **2/10/2026 4:23:00 AM**

Font: (Default) Times New Roman, 10 pt, English (United States)

Page 6: [65] Formatted **Cong Jiang** **2/10/2026 4:23:00 AM**

Font: (Default) Times New Roman, 10 pt, English (United States)

Page 6: [65] Formatted **Cong Jiang** **2/10/2026 4:23:00 AM**

Font: (Default) Times New Roman, 10 pt, English (United States)

Page 6: [66] Formatted **Cong Jiang** **2/10/2026 4:23:00 AM**

Font: (Default) Times New Roman, 10 pt, English (United States)

Page 6: [66] Formatted **Cong Jiang** **2/10/2026 4:23:00 AM**

Font: (Default) Times New Roman, 10 pt, English (United States)

Page 6: [67] Formatted **Cong Jiang** **2/10/2026 4:23:00 AM**

Font: (Default) Times New Roman, 10 pt, English (United States)

Page 6: [67] Formatted **Cong Jiang** **2/10/2026 4:23:00 AM**

Font: (Default) Times New Roman, 10 pt, English (United States)

Page 6: [68] Formatted **Cong Jiang** **2/10/2026 4:23:00 AM**

Font: (Default) Times New Roman, 10 pt, English (United States)

Page 6: [68] Formatted **Cong Jiang** **2/10/2026 4:23:00 AM**

Font: (Default) Times New Roman, 10 pt, English (United States)

Page 6: [69] Formatted **Cong Jiang** **2/10/2026 4:23:00 AM**

Font: (Default) Times New Roman, 10 pt, English (United States)

Page 6: [69] Formatted **Cong Jiang** **2/10/2026 4:23:00 AM**

Font: (Default) Times New Roman, 10 pt, English (United States)

Page 6: [70] Formatted **Cong Jiang** **2/10/2026 4:23:00 AM**

Font: (Default) Times New Roman, 10 pt, English (United States)

Page 6: [70] Formatted **Cong Jiang** **2/10/2026 4:23:00 AM**

Font: (Default) Times New Roman, 10 pt, English (United States)

Page 6: [71] Formatted **Cong Jiang** **2/10/2026 4:23:00 AM**

Font: (Default) Times New Roman, 10 pt, English (United States)

Page 6: [71] Formatted **Cong Jiang** **2/10/2026 4:23:00 AM**

Font: (Default) Times New Roman, 10 pt, English (United States)

Page 6: [72] Formatted **Cong Jiang** **2/10/2026 4:23:00 AM**

Font: (Default) Times New Roman, 10 pt, English (United States)

Page 6: [72] Formatted **Cong Jiang** **2/10/2026 4:23:00 AM**

Font: (Default) Times New Roman, 10 pt, English (United States)

Page 6: [73] Formatted **Cong Jiang** **2/10/2026 4:23:00 AM**

Font: (Default) Times New Roman, 10 pt, English (United States)

Page 6: [73] Formatted **Cong Jiang** **2/10/2026 4:23:00 AM**

Font: (Default) Times New Roman, 10 pt, English (United States)

Page 16: [74] Formatted **Cong Jiang** **2/10/2026 4:20:00 AM**

Font: 8 pt, Font color: Auto

Page 16: [75] Formatted **Cong Jiang** **2/10/2026 4:20:00 AM**

Font: 8 pt, Font color: Auto

Page 16: [76] Formatted **Cong Jiang** **2/10/2026 4:20:00 AM**

Font: 8 pt, Font color: Auto

Page 16: [77] Formatted **Cong Jiang** **2/10/2026 4:20:00 AM**

Font color: Auto

Page 16: [77] Formatted **Cong Jiang** **2/10/2026 4:20:00 AM**

Font color: Auto

Page 16: [78] Formatted **Cong Jiang** **2/10/2026 4:20:00 AM**

Font color: Auto

Page 16: [78] Formatted **Cong Jiang** **2/10/2026 4:20:00 AM**

Font color: Auto

Page 16: [79] Formatted **Cong Jiang** **2/10/2026 4:20:00 AM**

Font color: Auto

Page 16: [79] Formatted **Cong Jiang** **2/10/2026 4:20:00 AM**

Font color: Auto

Page 16: [80] Formatted **Cong Jiang** **2/10/2026 4:20:00 AM**

Font color: Auto

Page 16: [80] Formatted **Cong Jiang** **2/10/2026 4:20:00 AM**

Font color: Auto

Page 16: [81] Formatted **Cong Jiang** **2/10/2026 4:20:00 AM**

Font color: Auto

Page 16: [81] Formatted **Cong Jiang** **2/10/2026 4:20:00 AM**

Font color: Auto

Page 16: [82] Formatted **Cong Jiang** **2/10/2026 4:20:00 AM**

Font color: Auto

Page 16: [82] Formatted **Cong Jiang** **2/10/2026 4:20:00 AM**

Font color: Auto

Page 16: [83] Formatted **Cong Jiang** **2/10/2026 4:20:00 AM**

Font color: Auto

Page 16: [83] Formatted **Cong Jiang** **2/10/2026 4:20:00 AM**

Font color: Auto

Page 16: [84] Formatted **Cong Jiang** **2/10/2026 4:20:00 AM**

Font color: Auto

Page 16: [84] Formatted **Cong Jiang** **2/10/2026 4:20:00 AM**

Font color: Auto

Page 16: [85] Formatted **Cong Jiang** **2/10/2026 4:20:00 AM**

Font color: Auto

Page 16: [85] Formatted **Cong Jiang** **2/10/2026 4:20:00 AM**

Font color: Auto

Page 16: [86] Formatted **Cong Jiang** **2/10/2026 4:20:00 AM**

Font: 8 pt, Font color: Auto

Page 16: [87] Formatted **Cong Jiang** **2/10/2026 4:20:00 AM**

Font color: Auto

Page 16: [87] Formatted **Cong Jiang** **2/10/2026 4:20:00 AM**

Font color: Auto

Page 16: [88] Formatted **Cong Jiang** **2/10/2026 4:20:00 AM**

Font color: Auto

Page 16: [88] Formatted **Cong Jiang** **2/10/2026 4:20:00 AM**

Font color: Auto

Page 16: [89] Formatted **Cong Jiang** **2/10/2026 4:20:00 AM**

Font color: Auto

Page 16: [89] Formatted **Cong Jiang** **2/10/2026 4:20:00 AM**

Font color: Auto

Page 16: [90] Formatted **Cong Jiang** **2/10/2026 4:20:00 AM**

Font color: Auto

Page 16: [90] Formatted **Cong Jiang** **2/10/2026 4:20:00 AM**

Font color: Auto

Page 16: [91] Formatted **Cong Jiang** **2/10/2026 4:20:00 AM**

Font color: Auto

Page 16: [91] Formatted **Cong Jiang** **2/10/2026 4:20:00 AM**

Font color: Auto

Page 16: [92] Formatted **Cong Jiang** **2/10/2026 4:20:00 AM**

Font color: Auto

Page 16: [92] Formatted **Cong Jiang** **2/10/2026 4:20:00 AM**

Font color: Auto

Page 16: [93] Formatted **Cong Jiang** **2/10/2026 4:20:00 AM**

Font color: Auto

Page 16: [93] Formatted **Cong Jiang** **2/10/2026 4:20:00 AM**

Font color: Auto

Page 16: [94] Formatted **Cong Jiang** **2/10/2026 4:20:00 AM**

Font color: Auto

Page 16: [94] Formatted **Cong Jiang** **2/10/2026 4:20:00 AM**

Font color: Auto

Page 16: [95] Formatted **Cong Jiang** **2/10/2026 4:20:00 AM**

Font color: Auto

Page 16: [95] Formatted **Cong Jiang** **2/10/2026 4:20:00 AM**

Font color: Auto

Page 16: [96] Formatted **Cong Jiang** **2/10/2026 4:20:00 AM**

Font color: Auto

Page 16: [96] Formatted **Cong Jiang** **2/10/2026 4:20:00 AM**

Font color: Auto

Page 16: [97] Formatted **Cong Jiang** **2/10/2026 4:20:00 AM**

Font: 8 pt, Font color: Auto

Page 16: [98] Formatted **Cong Jiang** **2/10/2026 4:20:00 AM**

Font color: Auto

Page 16: [98] Formatted **Cong Jiang** **2/10/2026 4:20:00 AM**

Font color: Auto

Page 16: [99] Formatted **Cong Jiang** **2/10/2026 4:20:00 AM**

Font color: Auto

Page 16: [99] Formatted **Cong Jiang** **2/10/2026 4:20:00 AM**

Font color: Auto

Page 16: [100] Formatted **Cong Jiang** **2/10/2026 4:20:00 AM**

Font color: Auto

Page 16: [100] Formatted **Cong Jiang** **2/10/2026 4:20:00 AM**

Font color: Auto

Page 16: [101] Formatted **Cong Jiang** **2/10/2026 4:20:00 AM**

Font color: Auto

Page 16: [101] Formatted **Cong Jiang** **2/10/2026 4:20:00 AM**

Font color: Auto

Page 16: [102] Formatted **Cong Jiang** **2/10/2026 4:20:00 AM**

Font color: Auto

Page 16: [102] Formatted **Cong Jiang** **2/10/2026 4:20:00 AM**

Font color: Auto

Page 16: [103] Formatted **Cong Jiang** **2/10/2026 4:20:00 AM**

Font color: Auto

Page 16: [103] Formatted **Cong Jiang** **2/10/2026 4:20:00 AM**

Font color: Auto

Page 16: [104] Formatted **Cong Jiang** **2/10/2026 4:20:00 AM**

Font color: Auto

Page 16: [104] Formatted **Cong Jiang** **2/10/2026 4:20:00 AM**

Font color: Auto

Page 16: [105] Formatted **Cong Jiang** **2/10/2026 4:20:00 AM**

Font color: Auto

Page 16: [105] Formatted **Cong Jiang** **2/10/2026 4:20:00 AM**

Font color: Auto

Page 16: [106] Formatted **Cong Jiang** **2/10/2026 4:20:00 AM**

Font color: Auto

Page 16: [106] Formatted **Cong Jiang** **2/10/2026 4:20:00 AM**

Font color: Auto

Page 16: [107] Formatted **Cong Jiang** **2/10/2026 4:20:00 AM**

Font color: Auto

Page 16: [107] Formatted **Cong Jiang** **2/10/2026 4:20:00 AM**

Font color: Auto

Page 16: [108] Formatted **Cong Jiang** **2/10/2026 4:20:00 AM**

Font: 8 pt, Font color: Auto

Page 16: [109] Formatted **Cong Jiang** **2/10/2026 4:20:00 AM**

Font color: Auto

Page 16: [109] Formatted **Cong Jiang** **2/10/2026 4:20:00 AM**

Font color: Auto

Page 16: [110] Formatted **Cong Jiang** **2/10/2026 4:20:00 AM**

Font color: Auto

Page 16: [110] Formatted **Cong Jiang** **2/10/2026 4:20:00 AM**

Font color: Auto

Page 16: [111] Formatted **Cong Jiang** **2/10/2026 4:20:00 AM**

Font color: Auto

Page 16: [111] Formatted **Cong Jiang** **2/10/2026 4:20:00 AM**

Font color: Auto

Page 16: [112] Formatted **Cong Jiang** **2/10/2026 4:20:00 AM**

Font color: Auto

Page 16: [112] Formatted **Cong Jiang** **2/10/2026 4:20:00 AM**

Font color: Auto

Page 16: [113] Formatted **Cong Jiang** **2/10/2026 4:20:00 AM**

Font color: Auto

Page 16: [113] Formatted **Cong Jiang** **2/10/2026 4:20:00 AM**

Font color: Auto

Page 16: [114] Formatted **Cong Jiang** **2/10/2026 4:20:00 AM**

Font color: Auto

Page 16: [114] Formatted **Cong Jiang** **2/10/2026 4:20:00 AM**

Font color: Auto

Page 16: [115] Formatted **Cong Jiang** **2/10/2026 4:20:00 AM**

Font color: Auto

Page 16: [115] Formatted **Cong Jiang** **2/10/2026 4:20:00 AM**

Font color: Auto

Page 16: [116] Formatted **Cong Jiang** **2/10/2026 4:20:00 AM**

Font color: Auto

Page 16: [116] Formatted **Cong Jiang** **2/10/2026 4:20:00 AM**

Font color: Auto

Page 16: [117] Formatted **Cong Jiang** **2/10/2026 4:20:00 AM**

Font color: Auto

Page 16: [117] Formatted **Cong Jiang** **2/10/2026 4:20:00 AM**

Font color: Auto

Page 16: [118] Formatted **Cong Jiang** **2/10/2026 4:20:00 AM**

Font color: Auto

Page 16: [118] Formatted **Cong Jiang** **2/10/2026 4:20:00 AM**

Font color: Auto